Engineering Structures 295 (2023) 116836

Contents lists available at ScienceDirect

Engineering Structures

journal homepage: www.elsevier.com/locate/engstruct

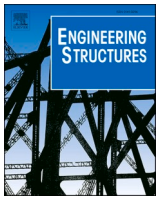

A model for the initial stiffness of the face plate component

Jorge Conde [b], Luis Simões da Silva [a,*], Ana Francisca Santos [a], Melaku Seyoum Lemma [a], Trayana Tankova [c]

[a] University of Coimbra, ISISE, ARISE, Department of Civil Engineering, Portugal
[b] Universidad Politécnica de Madrid, Departamento de Física y Estructuras de Edificación, Spain
[c] Technical University of Delft, Department of Engineering Structures, Netherlands

ARTICLE INFO

Keywords:
Component method
Connections
Face plate component
Minor axis joints
Eurocode 3

ABSTRACT

The component method for joint analysis relies on the formulation of stiffness and strength of individual parts to derive the global properties of the joint. One of these components is the web of an open I-section, or the face of a rectangular hollow section, hereby referred to as face plate. It is currently not codified despite its frequent occurrence in the engineering practice. Hereby, a new mechanical model is proposed to estimate the initial stiffness of the face plate component under out-of-plane loading, leading to closed-form analytical expressions. The model is validated against experimental test results and an extensive numerical parametric study, showing excellent agreement.

1. Introduction

The connection of steel members to the web of an open I-section, or the face of a rectangular hollow section, is characterized by the significant flexibility of the webs and face. This occurs due to the absence of a central stiffening element such as the web that is present in connections to the flanges of I-sections. This flexibility needs to be considered in the design of joints that present this active component [3]. Despite its practical relevance, Eurocode 3 part 1–8 [1], (EC3-1–8), does not contemplate this situation. Focusing on beam-to-column joints, Fig. 1 and Fig. 2 illustrate several joint typologies that share this component, henceforth referred to as "face plate", with various levels of demand, depending on the internal forces that are being transferred to the column.

If only shear force transfer is desired, the fin plate connection illustrated in Fig. 1(a) and Fig. 2(a) is usually the preferred solution because of its ease of fabrication, erection (due to the straightforward positioning of the beam) and good tolerances. In addition, the new FprEN 1993-1-8 [2], hereinafter referred to as FprEC3-1–8, provides guidance for fin plate joints connecting H- and I-sections in its Annex C, but only when connected to the column flange. Concerning RHS columns, no guidance is provided although the guidelines for welded T-joints in lattice structures connecting H- and I-sections through longitudinal plates to RHS chords could be adapted with respect to the chord resistance, but nothing is stated about the flexibility of these joints.

In many cases, because some degree of fixity at the beam ends has a very favorable impact on the design of the beam and the control of deflections, partial moment transfer in addition to shear transfer is desired and endplate joints (Fig. 1(b) and Fig. 2(b)) are used. Again, neither EC3-1–8, nor FprEC3-1–8, give any guidance for these cases. Although not illustrated in Fig. 1 and Fig. 2, direct connection to the chord faces is also present in many joint configurations in welded lattice structures. Their design is covered in clause 7 of EC3-1–8 but only from a resistance point of view with an implicit deformation criterion built-in in a semi-empirical way.

The joint typologies illustrated in Fig. 1 and Fig. 2 transfer forces from the beam to the column web/face in several ways depending on the specific connection detail. These vary from forces transferred by a plate welded to the web face, by direct contact over a certain area or by pulling associated with the contact from a bolt head or nut. Depending on the joint typology and the geometry of the connecting plate, the transferred load may be a force (exerted inwards or outwards) or a bending moment over a certain length, usually associated with the vertical shear force. Following the philosophy of the component method, the overall behavior for any of these situations can be obtained by analytical assembly of the individual components involved. Regarding the face plate of width b and thickness t, illustrated in Fig. 3(a), the component behavior is highly dependent on the way the load is applied, with the following basic cases: face plate connected to a single bolt row in tension, Fig. 3(b)(c)(d); face plate connected to a horizontal plate in tension or compression, Fig. 3(e); and face plate connected to a

* Corresponding author at: Civil Engineering Department, University of Coimbra, 3030-799 Coimbra, Portugal.
E-mail address: luisss@dec.uc.pt (L. Simões da Silva).

https://doi.org/10.1016/j.engstruct.2023.116836
Received 26 May 2023; Received in revised form 3 August 2023; Accepted 28 August 2023
Available online 2 September 2023

Nomenclature

A_v	shear area
B	axial force in bolt
E	Young's modulus
F	transverse force from fin plate or horizontal plate
F_{pl}	plastic resistance
G	shear modulus
I	moment of inertia
K_{ini}	initial stiffness
K_m	membrane stiffness
L_{eff}	length of equivalent strip
b	width of face plate
b_{hp}	width of horizontal plate
c	length of area of patch load
d	width of area of patch load
d_m	equivalent diameter of bolt head
e	width of beam
f_y	yield strength
h_{hp}	depth of fin plate
k	stiffness of the elastic foundation per unit length
n	distance between the bolt axis and the edge of the face plate; distance between the edge of a horizontal plate and the edge of the face plate; distance between the axis of a fin plate and the edge of the face plate;
p	bolt pitch
s	rotational stiffness per unit length of face plate longitudinal supports
t	thickness of face plate
t_{fp}	thickness of fin plate
t_{hp}	thickness of horizontal plate
α	ratio between the length of the area of the patch load and the width of face plate
β	ratio between the width of the area of the patch load and the width of face plate
θ	dispersion angle
μ	ratio between the width of face plate and the thickness of the face plate
ν	Poisson coefficient
f_y	yield strength

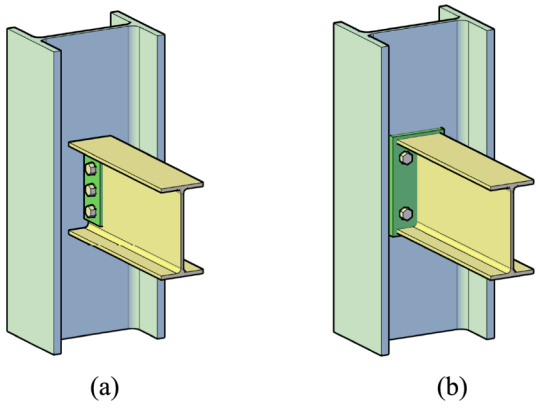

Fig. 1. Typical cases of connections to the web of an I section: (a) fin plate; (b) end plate.

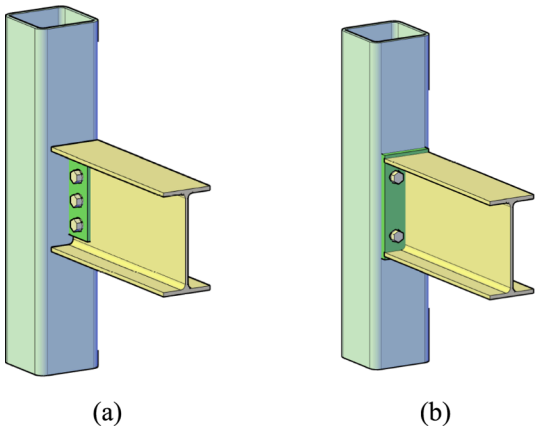

Fig. 2. Typical cases of connections to the face of a tube: (a) fin plate; (b) end plate.

fin plate in tension or compression, Fig. 3(f). These sub-figures introduce the basic notation used across the paper.

All the cases shown in Fig. 1 and Fig. 2 present a common feature, namely, the presence of a plate subjected to transverse tension or compression, which generally is slender (and therefore very flexible) with respect to the applied force. This component is supported on its vertical edges, with a variable degree of rotational stiffness imposed by the concurrent plates (for the joints presented in Fig. 1 the flanges of the open-section column, whereas for the joints in Fig. 2 the lateral faces of the hollow section). Moreover, these restraining elements also impose a variable degree of in-plane restraint, whereupon membrane forces develop, strongly contributing to the resistance and deformability of the plate. Finally, it must be considered that the plate is embedded in the column and therefore participates in the overall deformation and resistance of the frame.

The force–displacement behavior of the face plate component subjected to transverse force can be characterized by three regions (Fig. 4):

- the initial (elastic) region, dominated by plate bending, defined by the initial stiffness K_{ini} and extending up to the plastic resistance F_{pl};
- the last region is defined by the membrane stiffness K_m, which dominates the behaviour at a displacement u of the order of the plate thickness t.
- In between, a transition region where the plate response progressively changes from bending-type behaviour to membrane-type behaviour.

This paper focuses on the initial stiffness of the face plate component. This value is relevant because for most of its working life the joint remains within the elastic range, and therefore, its rotational behavior is dominated by the initial stiffness. Besides, an accurate characterization of this parameter is the first step of a full description of the force – displacement curve of the component. Hence, first, a short literature review on the topic is presented, followed by the derivation of a closed-form solution of the problem. The formulation is comprehensively validated against the results of a wide range of numerical results. Finally, the expressions are successfully compared to recent experimental results.

2. Literature review

2.1. Introduction

There are limited options available for estimating the initial stiffness of out-of-plane loaded chords using analytical formulations. Solutions of

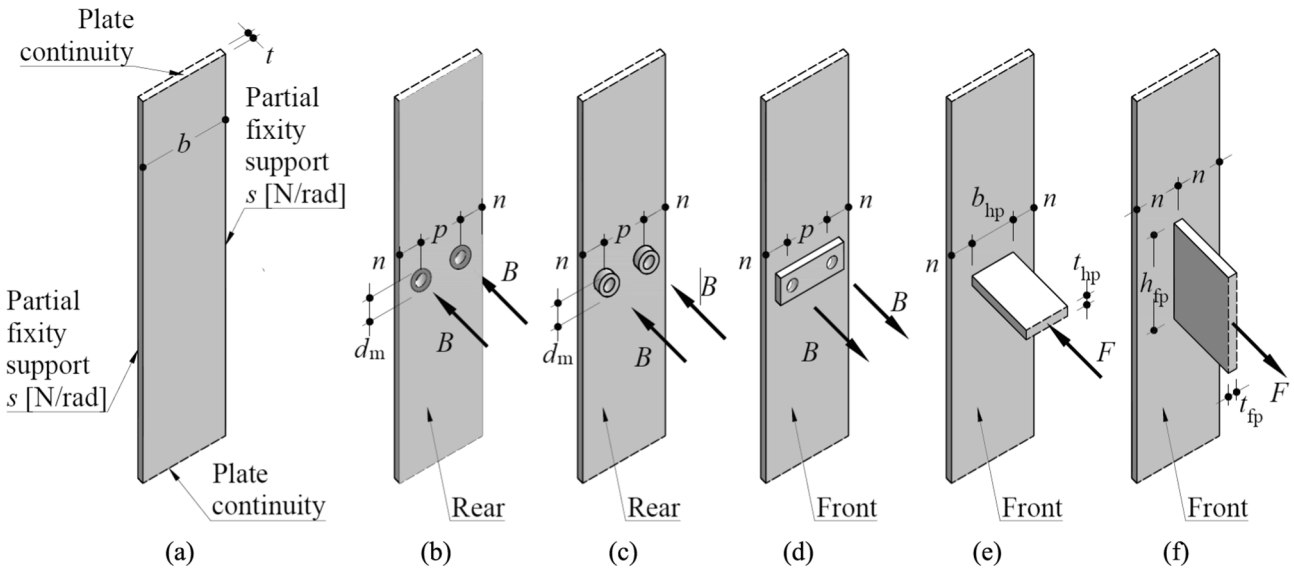

Fig. 3. Types of load application on a web/faced loaded with out-of-plane axial force: (a) face plate properties; (b)(c)(d) bolt row with end plate; (e) horizontal plate; (f) fin plate.

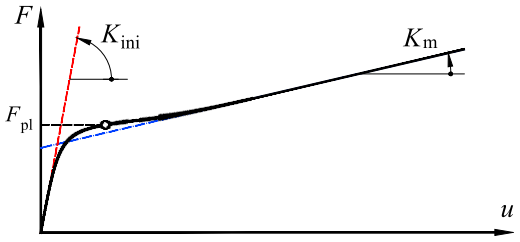

Fig. 4. Typical force−displacement curve on a web/faced loaded out-of-plane.

the differential equations of a rectangular plate subject to a transverse patch load are available but they usually consist of Fourier series solutions that require a significant number of terms to achieve reasonable accuracy [12,17]; hence, they are not useful for engineering practice. Consequently, most authors have proposed simplified expressions based on beam strip models, numerically calibrated for a specific range of validity. In the following sub-sections, they are briefly reviewed.

2.2. Previous studies

2.2.1. Neves et al

Neves [7] conducted tests on various end-plate beam-to-column joint specimens connecting I-section beams to both bare steel and infilled composite I-section columns and to concrete-filled tubular columns, subjected to monotonic and cyclic actions. Based on earlier numerical simulations and a simple equivalent strip analytical model [8], the initial stiffness of the column web in bending when subjected to a transverse load applied on a rigid area was derived using an equivalent strip model of length L_{eff}, as shown in Fig. 5(a) for an infinite plate of span b and thickness t, supported on its long edges, with partial

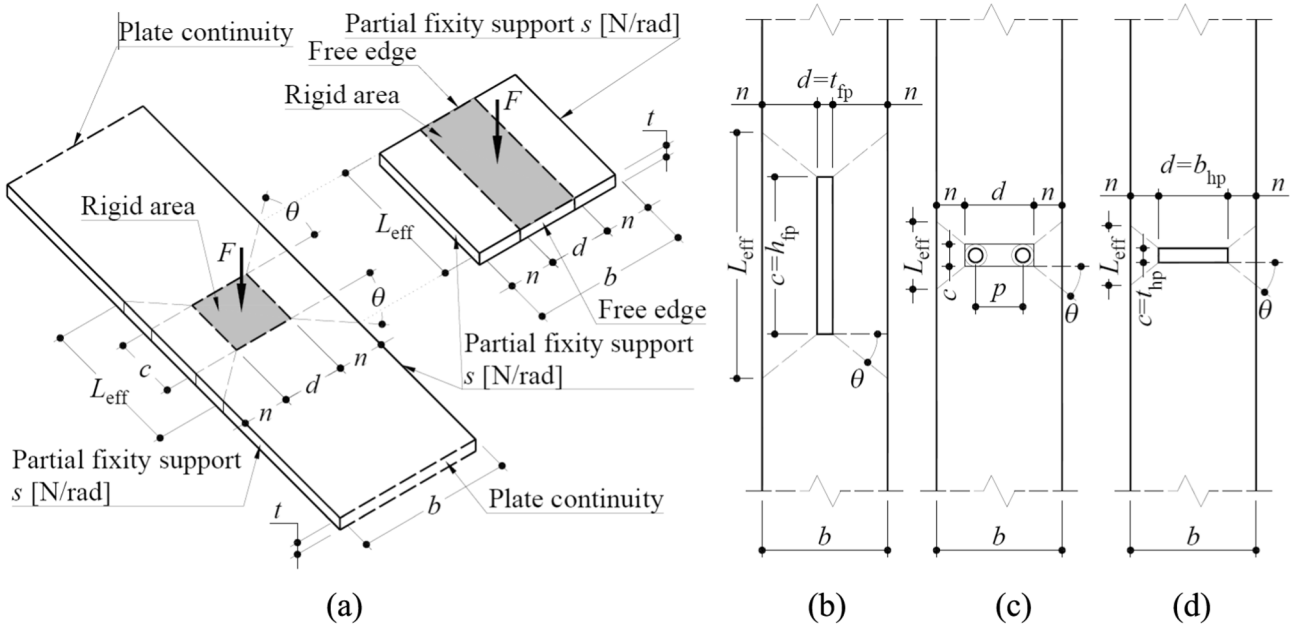

Fig. 5. Neves model and application to practical cases.

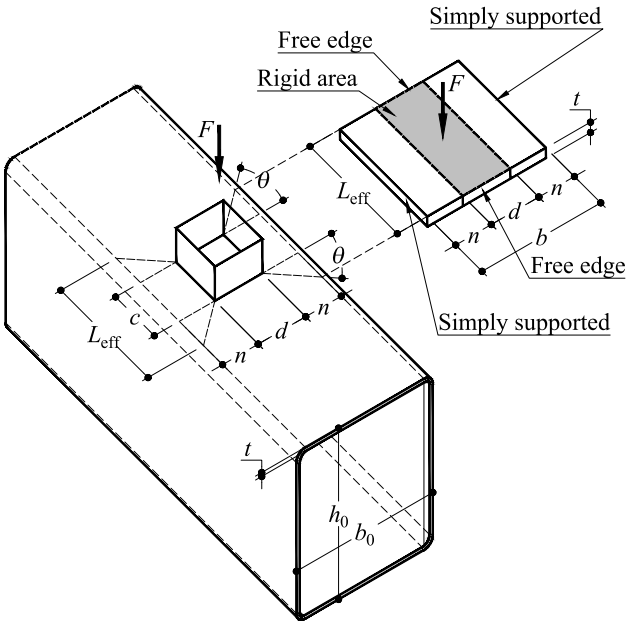

Fig. 6. Model for chord face in bending according to Garifulli *et al.* [13].

rotational stiffness per unit length s (N·mm/rad/mm); the load is applied as a patch load on an area $c \times d$, leaving two unloaded areas on the edge of length $n = (b - d)/2$. The model can be used for cases where the transverse load is applied through a horizontal plate (Fig. 5(b)), bolts (Fig. 5(c)), or a fin plate (Fig. 5(d)).

The model can be described with non-dimensional geometric parameters, $\alpha = c/b$, $\beta = d/b$, $\mu = b/t$. For fixed edges, taking the Poisson's ratio as $\nu = 0.3$, and introducing two coefficients $k_1 = 1.5$, and $k_2 = 1.63$ that were calibrated against the results of a numerical study, the following expression was obtained:

$$K_{ini,NEVES,fixed} = 16\frac{E\,t^3}{b^2}\frac{\alpha + (1-\beta)\tan\theta}{(1-\beta)^3 + 10.4\frac{k_1 - k_2\beta}{\mu^2}} \tag{1}$$

The term $10.4\cdot(k_1 - k_2\beta)/\mu^2$ is a correction for shear deformability in thick webs, and θ is a dispersion angle as shown in Fig. 5(a). Similarly, for partially restrained edges, the following expression was derived, not including shear deformation:

$$K_{ini,NEVES,partial} = 4\frac{E\,t^3}{b^2}\frac{\alpha + (1-\beta)\tan\theta + 6S\frac{1-\beta}{E\,t^3}}{(1-\beta)^3\left[1 + \frac{3S}{2}\frac{1-\beta}{E\,t^3(\alpha+(1-\beta)\tan\theta)}\right]}, \tag{2}$$

where S is the flexural rigidity of the boundary supports along the length L_{eff}:

$$S = s\,L_{eff} = s[c + 2n\tan(\theta)]. \tag{3}$$

The angle θ was calibrated to the results of a parametric study [8] yielding:

$$\theta = \begin{cases} 35 - 10\beta, & \beta < 0.7 \\ 49 - 30\beta, & \beta \geqslant 0.7 \end{cases} \tag{4}$$

The validity range for the expressions is limited to the cases depicted in Fig. 5(c) and Fig. 5(d) and $10 \leq \mu \leq 50$, $0.08 \leq \beta \leq 0.75$, $0.05 \leq \alpha \leq 0.20$. For the face plate loaded by a row bolt, the author suggests the use of an equivalent rectangular area with $d = p + d_m$ and $c = d_m$, where d_m is the mean of the across points and across flats dimensions of the bolt head or nut.

2.2.2. Park

Jaspart *et al.* [9] adopted the proposal by Neves in a paper that contemplates the use of the component method for joints in tubular construction. However, Park [10,11] suggested that the formulations by Jaspart *et al.* for hollow sections have a limited range of application and also pointed out that the expressions cannot be applied for connections with more than two bolt rows. Furthermore, this author presented analytical equations with improved accuracy and practicality by treating each bolt row as one joint component and allowing for their application with multiple bolt rows to estimate the initial stiffness, strength, and deformation capacity properties of joints to Rectangular Hollow Section (RHS) columns. The initial stiffness expression, proposed for each bolt row of a chord in transverse tension for hollow section columns with no concrete filling, is as follows:

$$K_{ini,PARK} = E\frac{f_1\,t^3}{b^2 m\cos\left(\frac{n\pi}{2b}\right)}, \tag{5}$$

where f_1 and m are adimensional parameters given by:

$$f_1 = \frac{11.5\,b\,k_r + 5.7\,E\,t^3 \times 1\text{mm}}{2.024\,b\,k_r\,m - b\,k_r + E\,m\,t^3 \times 1\text{mm}}, \tag{6}$$

$$k_r = \frac{4EI}{h}\left(\frac{1.5b + h}{2.0b + h}\right) = \frac{Et^3}{3h}\left(\frac{1.5b + h}{2.0b + h}\right), \tag{7}$$

$$m = 0.143\left(\frac{n}{b}\right)^2 - 0.306\left(\frac{n}{b}\right) + 1.076. \tag{8}$$

In these expressions, EI is the unit length bending stiffness of the plate, h is the depth of the RHS (measured orthogonally to the face plate), and all other parameters have already been defined. The expression is limited to hollow sections.

2.2.3. Garifullin et al.

Concluding that the range of applicability of the formulations by Neves [7] is very limited for the application to tubular T-joints, Garifullin *et al.* [13] proposed a simplified formulation for tube face in bending through a 2D beam analysis of a simply supported equivalent strip, see Fig. 6, assuming simple supports with no partial rotational stiffness.

The study first obtained the only unknown parameter, the effective length, from finite element analyses and finally suggested an expression using the numerical results. The reported range of validity is $0.25 \leq \beta \leq 0.85$, $0.5 \leq \alpha \leq 2.0$ and $10 \leq 2\gamma \leq 35$, where $\beta = d / b_0$, $\alpha = c / d$ and $2\gamma = b_0 / t$.

$$K_{ini,GARIFULLIN} = E\frac{4L_{eff}\,t^3}{(b-d)^3}, \tag{9}$$

$$L_{eff} = c(2 - \beta) + 1.25b_0(1 - \beta). \tag{10}$$

2.2.4. Ghobarah et al. [14] and Mahmood et al. [15]

Gohbarah *et al.* [14] studied hollow sections numerically and proposed a deflection coefficient to estimate the face plate deflection at the bolt locations, starting from a simply supported plate with two row bolts and subsequently applying correction factors. Mahmood *et al.* [15] found that the bolt pitch does not significantly affect the stiffness, and therefore the formulation by Gohbarah can be specified for a single bolt row. The corresponding expression is:

$$K_{ini,Ghobahra} = \frac{Et^3}{24\,\gamma_f(b - 2t)^2(1 - \nu^2)}. \tag{11}$$

where γ_f is a numerical coefficient dependent on μ (=b/t) and $\beta = n/(b - 2t)$. This coefficient is given graphically [15] for μ between 25–40, and β between 0.28–0.63. The range of available values of γ_f is small.

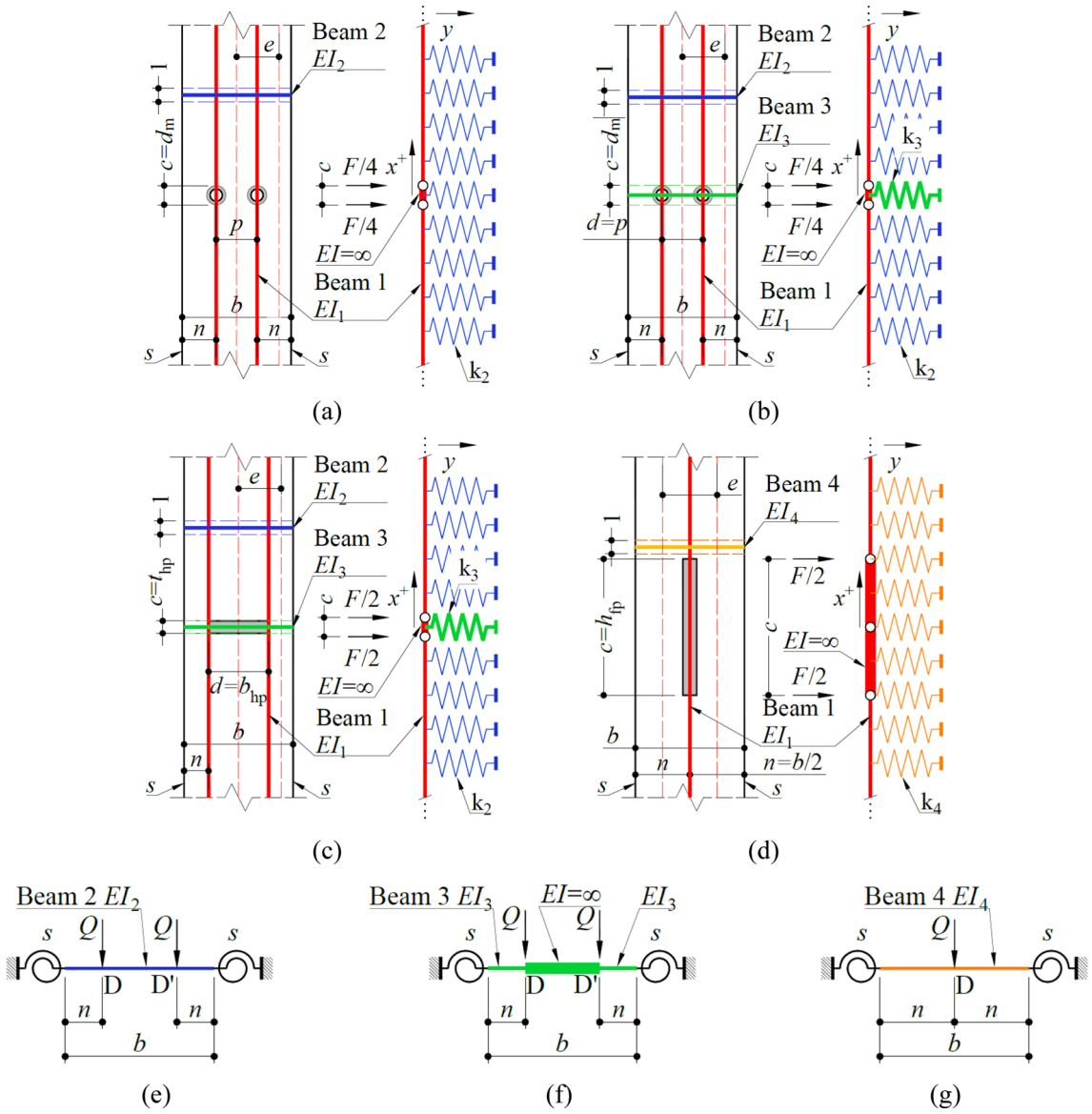

Fig. 7. Notation for grid model for face plate loaded by: (a) infinitely flexible bolted end plate; (b) infinitely rigid bolted end plate; (c) horizontal plate; (d) fin plate; (e) model for transverse beam 2; (f) model for transverse beam 3; (g) model for transverse beam 4.

3. Mechanical model for the initial stiffness

3.1. Introduction

The bending formulation of plate elements contains torsional components that are not present in a beam formulation and introduce additional complexity in the analytical solutions. A classical simplified approach to plate bending is the use of grid models composed of intertwined beams in two orthogonal directions [16] that neglect torsional stiffness. Consequently, they are supposed to yield a lower-bound solution, that is, smaller stiffness and resistance than the original plates, thus being on the safe side from an engineering point of view. This philosophy is applied to the face plate in this section. Moreover, because the face plate is assumed with infinite length, the corresponding parallel (infinite) grid beams can be considered as supported by the transversal grid beams and can be studied using the beam on elastic foundation theory [5], providing convenient closed-form solutions. The three canonic cases shown in Fig. 3(b)–(f), namely, face plate loaded by:

- a bolt row (two bolts per row) in tension, Fig. 3(b)(c)(d);
- a horizontal plate in tension or compression, Fig. 3(e);
- a fin plate in tension or compression, Fig. 3(f);

are treated with this rationale hereby, and the corresponding solutions are presented in the following sub-sections, using the unified notation of Fig. 3. In all cases, the face plate is transformed into a grid formed by a principal beam (referred to as 'beam 1') with total stiffness EI_1 (kN·mm^2) supported on an elastic foundation provided by the secondary beams (referred to as 'beam 2', 'beam 3', or 'beam 4'), see Fig. 7. The stiffness k (kN/mm^2) of the elastic foundation (per unit length) is found by analysis of the secondary beams of unit width and unit stiffness $EI_2 = EI_3 = EI_4$ (kN·mm^2/mm), with the appropriate boundary conditions, represented by the support flexibility per unit length s (kN·mm/rad/mm). Assuming that, for the applied load Q (kN/mm), the displacement at point D is d_D (mm), the corresponding stiffness is:

$$k_D = \frac{Q}{d_D}, \tag{12}$$

given in kN/mm^2. The displacement can be calculated excluding or including shear deformability of the plate. For all cases, the face plate

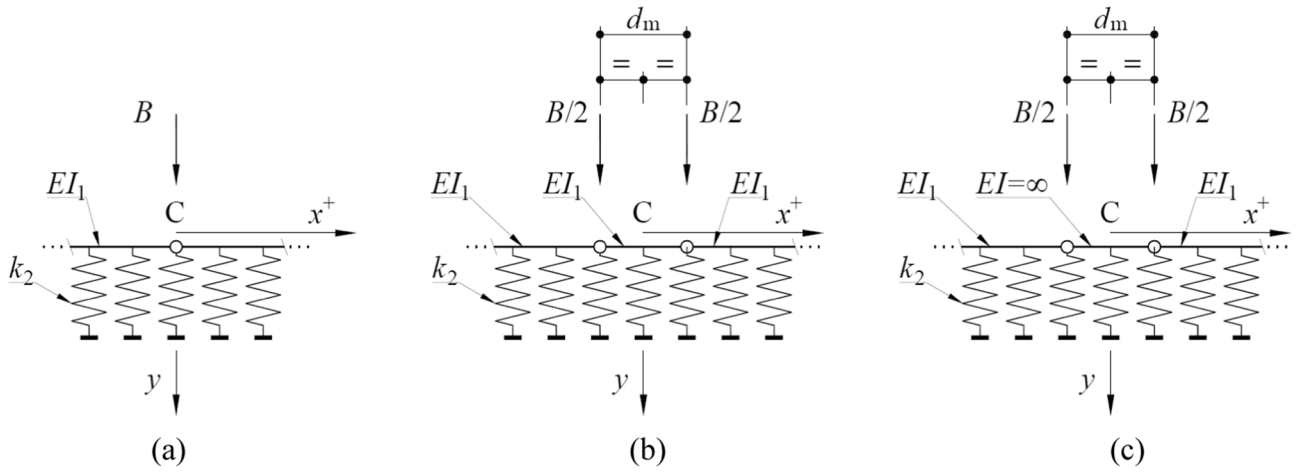

Fig. 8. Static model of beam 1 (beam on elastic foundation): (a) load applied as a point load; (b) load applied as two point loads, deformable segment; (c) load applied as two point loads, rigid segment.

Table 1
Closed-form solutions for the initial stiffness of a face plate loaded by bolt row in tension.

Case A: Force applied as a point load	$K_{1,A} = 8EI_1\lambda^3$	(23)
	$K_{1,A,fixed} = \frac{E}{1-\nu^2}\frac{2}{3}et^3\left(\frac{3b}{2n^2e(2ab-3n^2)}\right)^{0.75}$	(24)
	$K_{1,A,pinned} = \frac{E}{1-\nu^2}\frac{2}{3}et^3\left(\frac{3}{2ne(3nb-4n^2)}\right)^{0.75}$	(25)
Case B: Force applied as two point loads, considering the loaded area as deformable	$K_{1,B} = \frac{2K_{1,A}}{1+\exp(-\lambda d_m)[\cos(\lambda d_m)+\sin(\lambda d_m)]}$	(26)
Case C: Force applied as two point loads, considering the loaded area as undeformable	$K_{1,C} = K_{1,A} + k_2 d_m.$	(27)

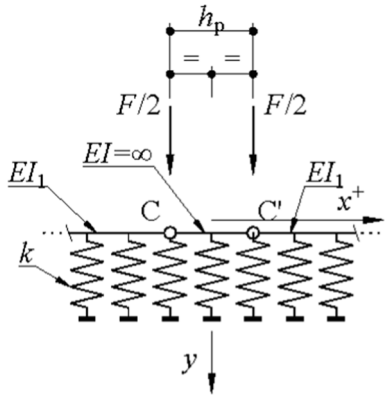

Fig. 9. Face plate supporting a fin plate. Model for beam 1.

with cross-section width b and plate thickness t, nominal material properties E (Young modulus), ν (Poisson coefficient) and f_y (yield strength), is assumed as infinite in the longitudinal direction. In-plane forces and second-order effects are disregarded. For the first case (face plate loaded by a bolt row), two extreme solutions are discussed, namely a very (infinitely) flexible bolted end plate, and a very (infinitely) rigid bolted end plate. Both sub-cases differ in the rotation restraint of the load application area (washer area), free for the former and fixed for the latter. The actual behavior of the connection is expected to lie in between both extremes, but experimental results (discussed further below) indicate that it is closer to the second.

3.2. Case 1a: Face plate loaded by infinitely flexible bolted end plate

3.2.1. Face plate in pure bending

Fig. 7(a) shows the frontal view of a plate face, loaded by two bolts in tension, with nominal bolt diameter d, and corresponding hole diameter d_0 (see also Fig. 3(b)(c)(d)). The corresponding bolted end plate is assumed as infinitely flexible, so that the loaded area is not restrained for rotation. The total load (transferred by the 2 bolts) is F. The load at each bolt, $B = F/2$, is transferred to the face plate by means of an annular surface of external diameter d_m. The cross-section of beam 1 is defined by the width e. This parameter can be adjusted to improve the accuracy of the method, but for simplicity it can be taken as approximately equal to $b/2$. The cross-section of beam 2 is defined by the thickness t and a unit width. Beam 1 can be assumed of infinite length if the column extends at least $2b$ at each side of the load application, that is, a minimum column length of $4b$ [14]. This assumption is therefore reasonable in buildings, except at column ends, or whenever transverse stiffeners are present.

The mechanical model corresponding to the transverse beams (beam 2) is shown in Fig. 7(e). Depending on the support stiffness s (kN·mm/rad/mm), three cases can be discussed: (a) the plate is fixed at the edges, $s = \infty$ kN/rad; (b) the plate is simply supported at the edges, $s = 0$ kN/rad; (c) the edges present an intermediate unit rotational stiffness s. The last case allows for calibration of the true support conditions of the plate, based on the cross-sectional properties of the column. The first and second cases correspond to upper and lower bounds of the stiffness. In this model, the attached bolts and end plates are infinitely flexible, so it is assumed that the bolt does not restrain the rotation of the plate at points D and D', therefore the model will, in theory, lead to a (conservative) lower bound of the real stiffness of the plate.

For the fixed case, $s = \infty$ kN/rad, the displacement d at point D is given by:

$$d_{D,fixed} = \frac{Qn^3}{6EI_2b}(2b - 3n), \tag{13}$$

where Q (kN/mm) is the unit load and

$$EI_2 = E\frac{t^3}{12(1-\nu^2)}, \tag{14}$$

whereupon the unit stiffness $k_{D,fixed}$ at point D is measured as:

$$k_{D,fixed} = \frac{6EI_2b}{n^2(2nb-3n^2)} = \frac{E}{1-\nu^2}\frac{bt^3}{2n^3(2b-3n)}. \tag{15}$$

In the previous expressions, Q and d are auxiliary magnitudes used

Table 2
Proposed equations to estimate the initial stiffness of a face plate component subjected to transverse load.

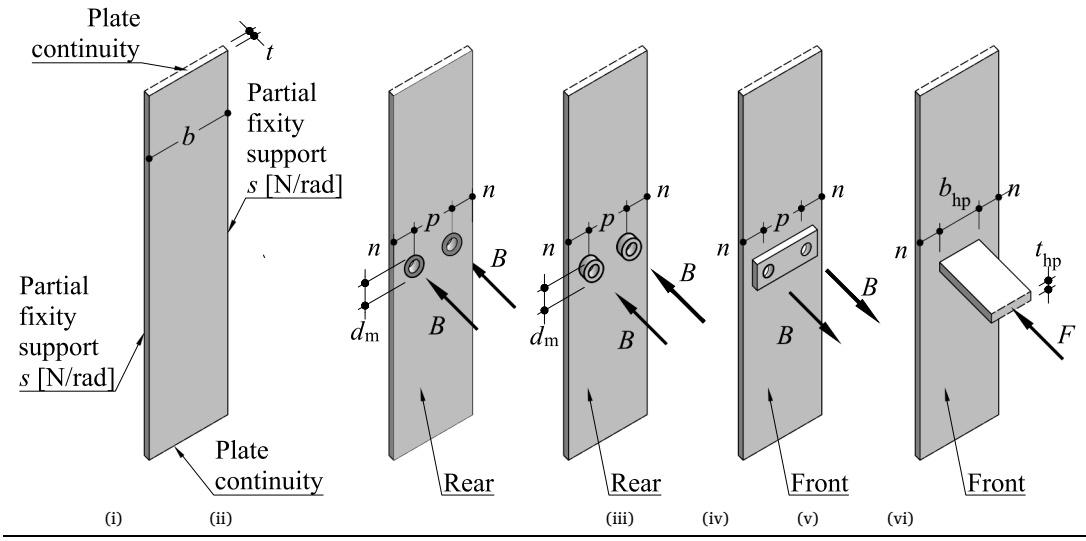

(i) face plate and boundary conditions; (ii) face plate loaded by infinitely flexible bolted end plate (rear view); (iii)(iv) face plate loaded by infinitely rigid bolted end plate (rear and front view); (v) face plate loaded by horizontal plate in tension or compression; (vi) face plate loaded by fin plate in tension or compression.

$K = r\left(8EI_1\lambda^3 + k_3 c\right), EI_1 = eEI_2, \lambda = (k_2/4EI_1)^{0.25}, EI_2 = Et^3/12(1-\nu^2), GA_v = 2Gt/3, k_2 = 1/d_2, k_3 = 1/d_3.$

case	r	e	c	d_2	d_3
(ii)(iv)	2	$b/2$	d_m	$\frac{n^3 s(2b-3n)+2EI_2 n^2(4n-3b)}{6EI_2(2EI_2+bs)} + \frac{n}{GA_v}$	$=d_2$
(iii)(iv)					$\frac{n^3}{12EI_2}\frac{sn+4EI_2}{sn+EI_2} + \frac{n}{GA_v}$
(v)			$t+t_{hp}$		
(vi)	1	b	h_{fp}	$\frac{b^3(8EI_2+bs)}{192EI_2(2EI_2+bs)} + \frac{b}{4GA_v}$	$= d_2$

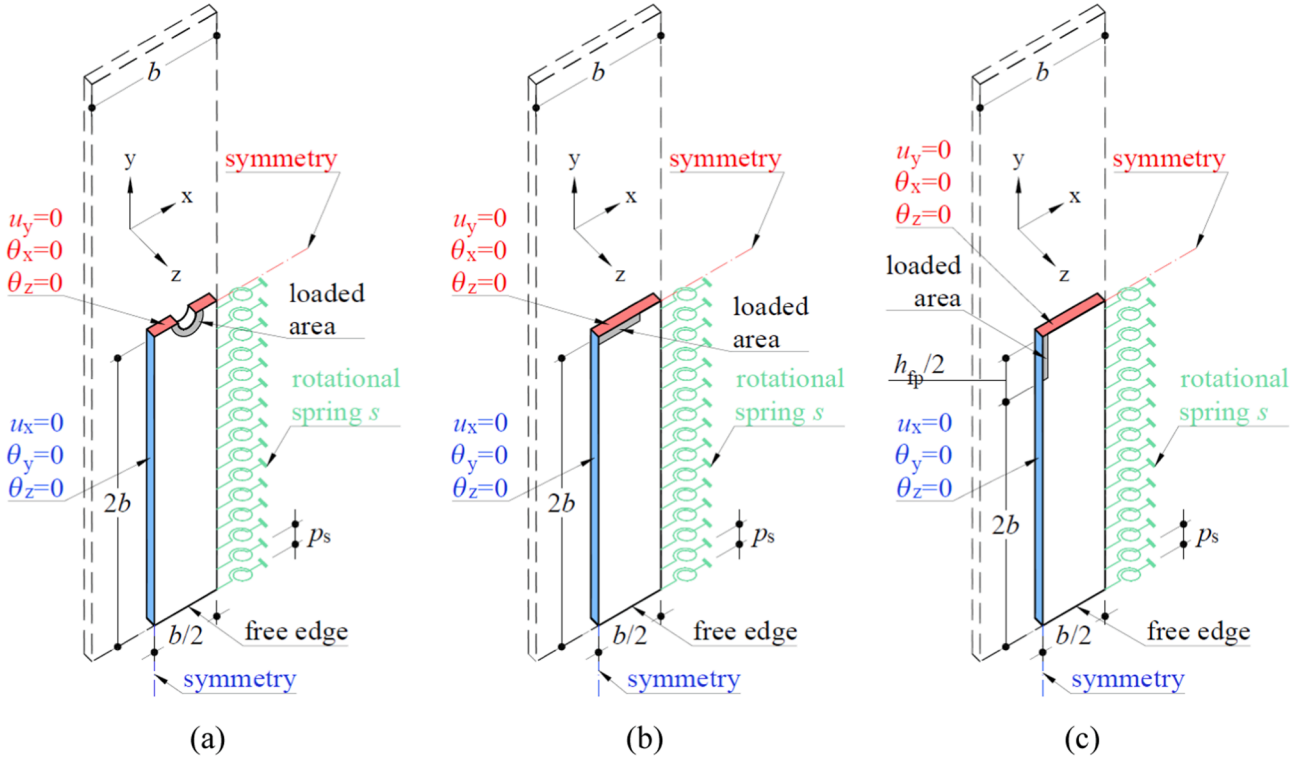

Fig. 10. General view of the FEM model for face plate loaded by: (a) bolted end plate (one bolt row); (b) horizontal plate; (c) fin plate.

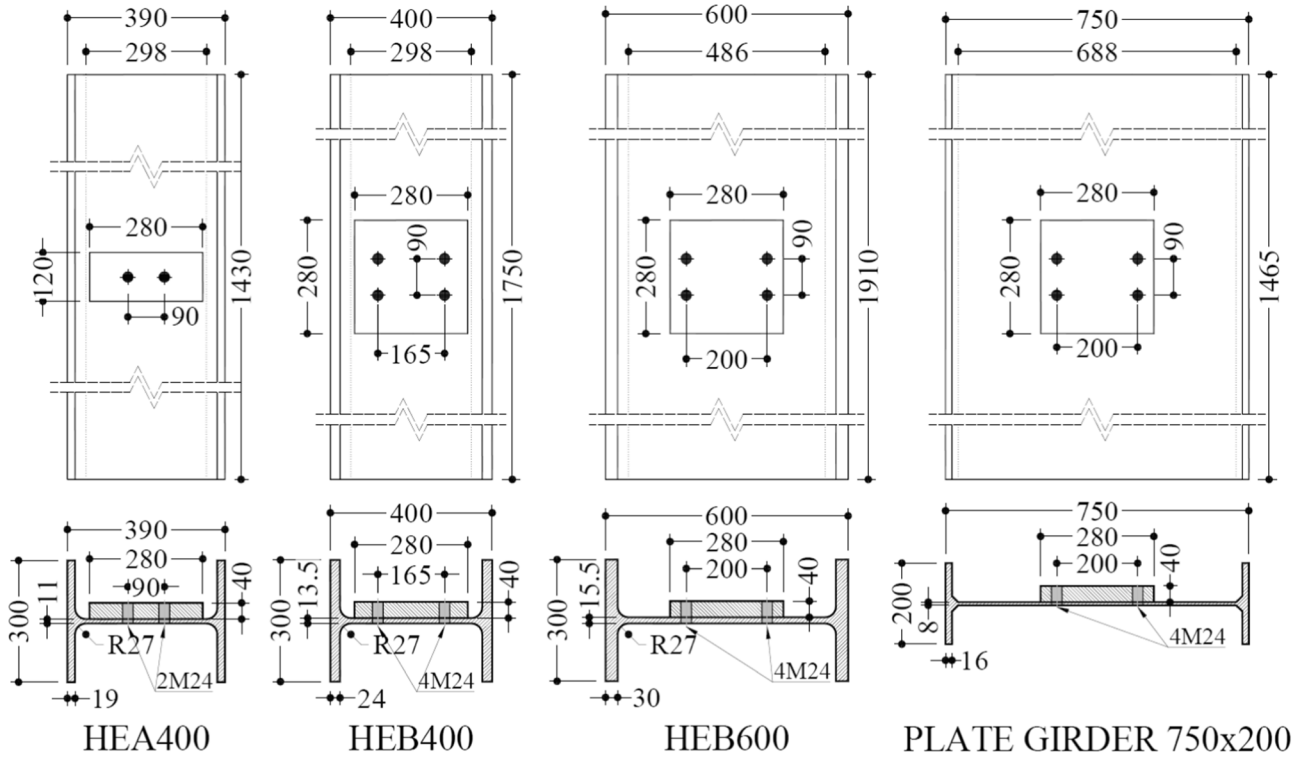

Fig. 11. Geometry of the tests.

Table 3
Estimate of initial stiffness.

Column		HE400A	HE400B	HE600B	W750x200
b	mm	306	301	483.2	701
t	mm	11	13.5	15.5	8
p	mm	90	165	200	200
d_m	mm	44	44	44	44
EI_2	kN·mm²/mm	25,596	47,315	71,613	9846
s_b	kN/rad	167.3	314.4	296.4	28.1
s	kN/rad	669.0	78.6	222.3	140.0
$\rho = s/s_b$		4	0.3	0.8	5.0
F	kN	27.2	60.7	38.5	17.5
u	mm	0.72	0.42	0.70	4.29
K	**kN/mm**	**37.7**	**144.5**	**55.2**	**4.1**
Neves model (Eq. (2))					
K_N	kN/mm	81.2	523.6	87.0	5.2
K_N/K	kN/mm	216%	362%	158%	128%
Proposed model, assuming rigid bolted end plate					
$K_{C,V,rigid}$	**kN/mm**	**47.3**	**185.84**	**57.0**	**3.9**
$K_{C,V,rigid}/K$	kN/mm	125%	129%	103%	96%
Proposed model, assuming flexible bolted end plate					
$K_{C,V,flexible}$	kN/mm	41.8	89.6	40.94	3.4
$K_{C,V,flexible}/K$	kN/mm	111%	62%	74%	83%

only to obtain the stiffness. Likewise, for the simply supported case:

$$k_{D,pinned} = \frac{6EI_2}{n(3nb - 4n^2)} = \frac{E}{1-\nu^2}\frac{t^3}{2n^2(3b-4n)}. \quad (16)$$

In the former expressions, the subscript 'pinned' is used to identify the simply supported case. Finally, for the partial fixity, identified with the subscript 'partial':

$$k_{D,partial} = \frac{6EI_2(2EI_2 + bs)}{n^3 s(2b-3n) + 2EI_2 n^2(3b-4n)} = \frac{E}{1-\nu^2}\frac{t^3(Et^3 + 6sb(1-\nu^2))}{2n^2[6sn(1-\nu^2)(2b-3n) + Et^3(3b-4n)]}. \quad (17)$$

Derivation of this expression is given in Appendix A. If $s = 0$, the expression reduces to Eq. (16), whereas for $s = \infty$, Eq. (15) is obtained. Eq. (17) represents the unit stiffness of the supporting element for beam 1 in Fig. 7(a), and therefore the behavior of beam 1 can be assimilated to an infinite beam on elastic foundation of unit stiffness $k_2 = k_D$, subjected to the point load $B = F/2$ corresponding to one bolt, as shown in Fig. 8, where three different possibilities are presented, depending on the load application: in Fig. 8(a) the load B is applied at one point (Case A); in Fig. 8(b), the area of load application is considered as deformable (Case B); finally, in Fig. 8(c), the area of load application is considered of infinite stiffness (case C). The derivation for each case, based on [5], is given in Appendix A. Hereby, only the main equations are summarized.

The stiffness EI_1 of beam 1 is:

$$EI_1 = E\frac{e\,t^3}{12(1-\nu^2)}. \quad (18)$$

As indicated, the width e must be chosen, with a maximum geometrical value of $b/2$. The behavior of the system is dependent on the parameter λ (see Appendix A), defined as:

$$\lambda = \left(\frac{k_2}{4EI_1}\right)^{0.25}, \quad (19)$$

which, applying Eqs. (15), (16) and (17) results in:

$$\lambda_{fixed} = \left(\frac{3b}{2en^3(2b-3n)}\right)^{0.25}, \quad (20)$$

$$\lambda_{pinned} = \left(\frac{3}{2en^2(3b-4n)}\right)^{0.25}, \quad (21)$$

Table 4
Results of parametric study for face plate loaded by an infinitely flexible bolted end plate.

Boundary condition	Statistic	Neves	Proposed method without shear correction			Proposed method with shear correction		
		K_N/K_{FE}	K_A/K_{FE}	K_B/K_{FE}	K_C/K_{FE}	$K_{A,V}/K_{FE}$	$K_{B,V}/K_{FE}$	$K_{C,V}/K_{FE}$
Fixed (48 cases)	Max	8.811	1.095	1.248	1.431	1.092	1.096	1.212
	Min	1.190	0.813	0.933	1.062	0.780	0.916	1.042
	Mean	2.100	1.004	1.042	1.137	0.987	1.023	1.115
	C.o.V.	70.8%	7.3%	5.7%	5.4%	8.2%	5.2%	3.3%
	R^2	–	0.996	0.949	0.831	0.988	0.997	0.956
Pinned (48 cases)	Max	6.952	0.908	0.911	0.957	0.907	0.910	0.954
	Min	0.708	0.635	0.681	0.771	0.632	0.678	0.766
	Mean	1.514	0.837	0.851	0.909	0.834	0.848	0.906
	C.o.V.	86.1%	8.1%	6.6%	4.4%	8.3%	6.8%	4.5%
	R^2	–	0.908	0.937	0.980	0.899	0.929	0.974
Partial fixity $\rho = 0.5, 1, 2$ (144 cases)	Max	5.859	0.997	0.999	1.037	0.995	0.998	1.035
	Min	0.926	0.641	0.695	0.789	0.636	0.690	0.783
	Mean	1.668	0.868	0.887	0.954	0.863	0.882	0.948
	C.o.V.	59.9%	8.8%	7.0%	4.9%	9.2%	7.4%	5.1%
	R^2	–	0.975	0.989	1.000	0.967	0.983	0.998
All (240 cases)	Max	8.811	1.095	1.248	1.431	1.092	1.096	1.212
	Min	0.708	0.635	0.681	0.771	0.632	0.678	0.766
	Mean	1.723	0.889	0.910	0.981	0.882	0.903	**0.973**
	C.o.V.	68.8%	10.6%	9.9%	9.5%	10.7%	9.6%	**8.8%**
	R^2	–	0.989	1.000	0.975	0.989	1.000	0.989

Table 5
Results of parametric study for face plate loaded by an infinitely stiff bolted end plate.

Boundary condition	Statistic	Neves	Proposal	
		K_N/K_{FE}	K_C/K_{FE}	$K_{C,V}/K_{FE}$
Fixed (48 cases)	Max	5.806	1.389	1.097
	Min	1.127	0.665	0.606
	Mean	1.507	0.974	0.945
	C.o.V.	53.2%	12.77%	11.37%
	R^2	–	0.868	0.988
Pinned (48 cases)	Max	3.614	0.913	0.913
	Min	0.685	0.437	0.427
	Mean	1.000	0.775	0.770
	C.o.V.	52.0%	13.53%	13.84%
	R^2	–	0.933	0.904
Partial fixity $\rho = 0.5, 1, 2$ (144 cases)	Max	3.331	0.997	0.996
	Min	0.885	0.441	0.430
	Mean	1.200	0.825	0.817
	C.o.V.	33.7%	13.15%	13.66%
	R^2	–	0.987	0.973
All (240 cases)	Max	5.806	1.389	1.097
	Min	0.685	0.437	0.427
	Mean	1.221	0.845	0.833
	C.o.V.	45.1%	15.35%	14.90%
	R^2	–	0.994	0.988

$$\lambda_{\text{partial}} = \left(\frac{3[Et^3 + 6sb(1-\nu^2)]}{2en^2[6sn(1-\nu^2)(2b-3n) + Et^3(3b-4n)]} \right)^{0.25}. \tag{22}$$

Again, the last expression, Eq. (22), reduces to Eq. (20) for $s = \infty$ kN/rad, and to Eq. (21) for $s = 0$ kN/rad. Choosing λ as corresponding, the closed-form solutions for each of the three cases shown in Fig. 8 are summarized in Table 1:

In the previous equations, k_2 (lower case) denotes unit stiffness (kN/mm/mm) whereas K (upper case) is used for stiffness (kN/mm), and the subscript '1′ indicates that this is for one of the two beams 'beam 1′. Thus, the total stiffness for the face plate component, K, is:

$$K_X = 2K_{1,X}, \tag{28}$$

where 'X' stands for A, B or C, and $K_{1,X}$ is $K_{1,A}$, $K_{1,B}$, or $K_{1,C}$ as chosen. $K_{1,A}$ is expected to lead to the most conservative (lowest) value, whereas $K_{1,C}$ will produce the less conservative (highest) value. The deformation Δ of the face plate component is given by:

$$\Delta_X = F/K_X. \tag{29}$$

where F is the total force corresponding to the two bolts, $F = 2B$.

3.2.2. Shear correction

Shear deformation can be included in the former expressions by correcting the beam stiffness. However, the largest part of the shear contribution is expected from beam 2 due to the reduced slenderness of this element. Thus, in the following derivation, shear deformation will only be considered in beam 2. This allows for an explicit solution (which is not possible if shear deformability is included in beam 1). The additional deformation of beam 2 due to shear at point D for any of the three boundary conditions is approximately given by [6]:

$$d_{D,V} = \frac{Qn}{GA_v}, \tag{30}$$

where $G = E/(2\cdot(1+\nu))$ is the shear modulus of the material and $A_V = 2\,t/3$ is the equivalent shear area of the rectangular cross-section per unit length. Thus, the total stiffness considering bending and shear deformation is:

$$k_D = \frac{Q}{d_{D,M} + d_{D,V}}, \tag{31}$$

where $d_{D,M}$ is the deflection due to pure bending of beam 2 under load Q, for the corresponding boundary conditions. This expression can be rewritten as:

$$k_D = \frac{Q}{d_{D,M}\left(1 + \frac{d_{D,V}}{d_{D,M}}\right)} = k_{D,M}\frac{d_{D,M}}{d_{D,V} + d_{D,M}} = k_{D,M}\beta_V, \tag{32}$$

Table B1
Parametric study cases – face plate loaded by bolted plate.

n	g (mm)	t (mm)	b (mm)	a (mm)	t/d	b/g	b/t	b/a	a/t
1	80	8	160	40	0.5	2.00	20	4.00	5.00
2	80	8	200	60	0.5	2.50	25	3.33	7.50
3	80	8	240	80	0.5	3.00	30	3.00	10.00
4	80	8	280	100	0.5	3.50	35	2.80	12.50
5	80	8	320	120	0.5	4.00	40	2.67	15.00
6	80	8	360	140	0.5	4.50	45	2.57	17.50
7	80	8	400	160	0.5	5.00	50	2.50	20.00
8	80	12	180	50	0.75	2.25	15	3.60	4.17
9	80	12	240	80	0.75	3.00	20	3.00	6.67
10	80	12	300	110	0.75	3.75	25	2.73	9.17
11	80	12	360	140	0.75	4.50	30	2.57	11.67
12	80	12	420	170	0.75	5.25	35	2.47	14.17
13	80	12	480	200	0.75	6.00	40	2.40	16.67
14	80	12	540	230	0.75	6.75	45	2.35	19.17
15	80	12	600	260	0.75	7.50	50	2.31	21.67
16	80	16	160	40	1	2.00	10	4.00	2.50
17	80	16	240	80	1	3.00	15	3.00	5.00
18	80	16	320	120	1	4.00	20	2.67	7.50
19	80	16	400	160	1	5.00	25	2.50	10.00
20	80	16	480	200	1	6.00	30	2.40	12.50
21	80	16	560	240	1	7.00	35	2.33	15.00
22	80	16	640	280	1	8.00	40	2.29	17.50
23	80	16	720	320	1	9.00	45	2.25	20.00
24	80	16	800	360	1	10.00	50	2.22	22.50
25	96	8	160	32	0.5	1.67	20	5.00	4.00
26	96	8	200	52	0.5	2.08	25	3.85	6.50
27	96	8	240	72	0.5	2.50	30	3.33	9.00
28	96	8	280	92	0.5	2.92	35	3.04	11.50
29	96	8	320	112	0.5	3.33	40	2.86	14.00
30	96	8	360	132	0.5	3.75	45	2.73	16.50
31	96	8	400	152	0.5	4.17	50	2.63	19.00
32	96	12	180	42	0.75	1.88	15	4.29	3.50
33	96	12	240	72	0.75	2.50	20	3.33	6.00
34	96	12	300	102	0.75	3.13	25	2.94	8.50
35	96	12	360	132	0.75	3.75	30	2.73	11.00
36	96	12	420	162	0.75	4.38	35	2.59	13.50
37	96	12	480	192	0.75	5.00	40	2.50	16.00
38	96	12	540	222	0.75	5.63	45	2.43	18.50
39	96	12	600	252	0.75	6.25	50	2.38	21.00
40	96	16	160	32	1	1.67	10	5.00	2.00
41	96	16	240	72	1	2.50	15	3.33	4.50
42	96	16	320	112	1	3.33	20	2.86	7.00
43	96	16	400	152	1	4.17	25	2.63	9.50
44	96	16	480	192	1	5.00	30	2.50	12.00
45	96	16	560	232	1	5.83	35	2.41	14.50
46	96	16	640	272	1	6.67	40	2.35	17.00
47	96	16	720	312	1	7.50	45	2.31	19.50
48	96	16	800	352	1	8.33	50	2.27	22.00

where $k_{D,M}$ is the stiffness considering only bending components and

$$\beta_V = \frac{d_{D,M}}{d_{D,V} + d_{D,M}}, \tag{33}$$

is the shear correction coefficient, indicative of the relative importance of shear deflection, when compared to pure bending deflection. Its closed-form expression for the fixed supported beam is:

$$\beta_{V,fixed} = 1 - \frac{3bt^2}{3bt^2 + 2n^2(1-\nu)(2b-3n)}. \tag{34}$$

For the simply supported beam:

$$\beta_{V,pinned} = 1 - \frac{3t^2}{3t^2 + 2n(1-\nu)(3b-4n)}. \tag{35}$$

Finally, for the partial fixity:

$$\beta_{V,partial} = \frac{1}{1 + \frac{3t^2[Et^3+6sb(1-\nu^2)]}{2n(1-\nu)[6sn(1-\nu^2)(2b-3n)+Et^3(3b-4n)]}}. \tag{36}$$

Again, in the previous derivations, Q and d are auxiliary magnitudes.

3.3. Case 1b: Face plate loaded in tension by infinitely rigid bolted end plate

This case is presented in Fig. 7(b). The formulation for beam 2 is identical to that of the previous case. A third beam of unit width and stiffness EI_3, referred to as 'beam 3′ and shown in Fig. 7(f), includes the local stiffening of the face plate due to the horizontal plate, by considering a central rigid region (with infinite stiffness). The model for beam 1 presented as case C in Section 3.2, see Fig. 8(c), can be applied, but the stiffness below the central rigid area of the beam is k_3 (kN/mm^2) instead of k_2. Eq. (27) can be reformulated as:

$$K_1 = 8EI_1\lambda^3 + k_3\, c, \tag{37}$$

$$K = 2K_1, \tag{38}$$

where c is the width where beam 3 is considered, as shown in Fig. 7(b). It can be taken as d_m for simplicity. The stiffness $k_3 = k_D$ for the fixed, pinned and partial fixity, can be obtained as:

$$k_{D,fixed} = \frac{12EI_3}{n^3} = \frac{E}{1-\nu^2}\frac{t^3}{n^3}, \tag{39}$$

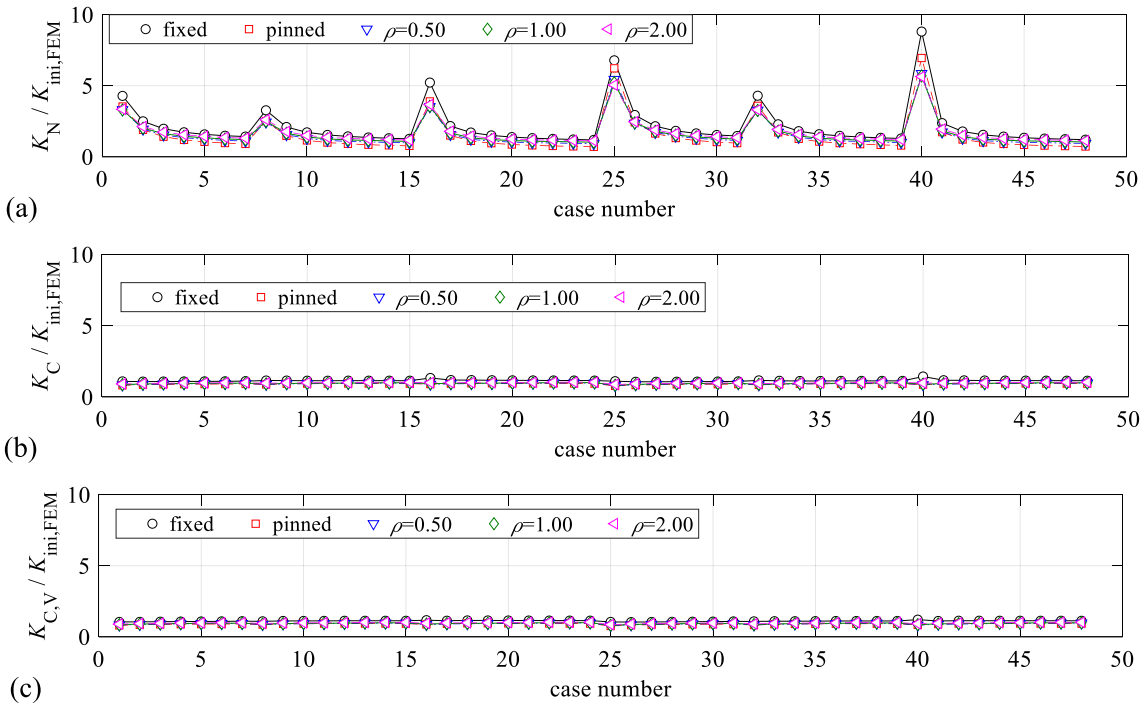

Fig. 12. Verification of the proposed methods for face plate loaded by an infinitely flexible bolted end plate: (a) K_N (Neves); (b) K_C; (c) $K_{C,V}$.

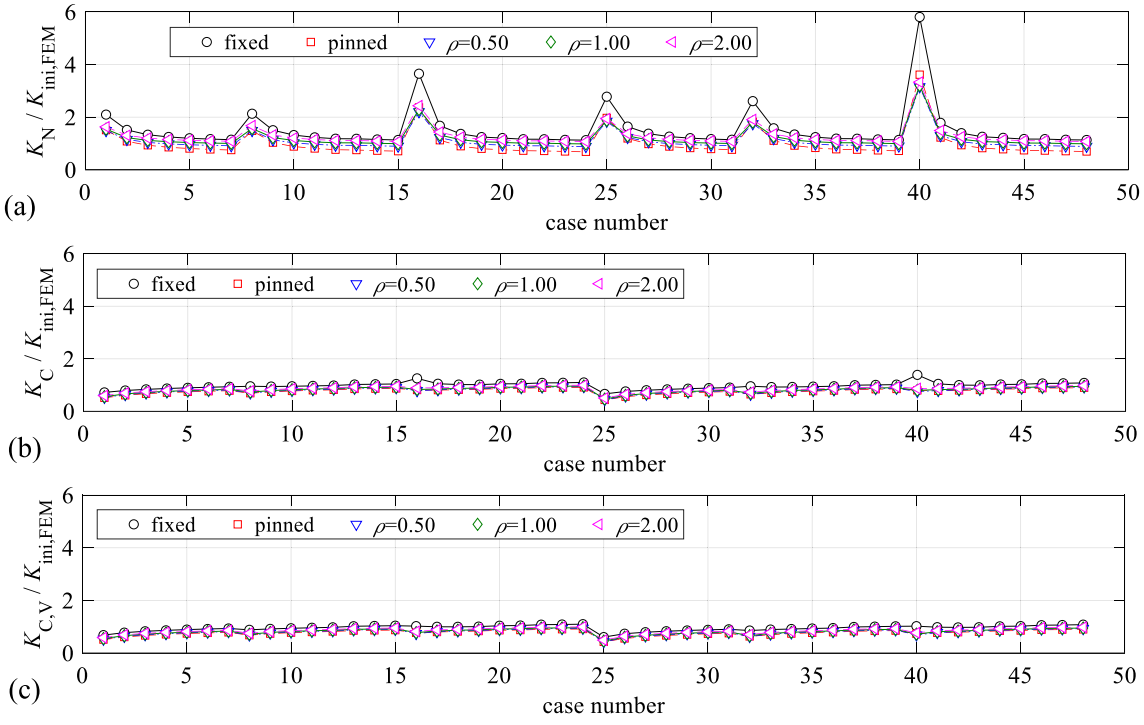

Fig. 13. Verification of the proposed methods for face plate loaded by an infinitely stiff bolted end plate: (a) K_N (Neves); (b) K_C; (c) $K_{C,V}$.

$$k_{D,pinned} = \frac{3EI_3}{n^3} = \frac{E}{1-\nu^2}\frac{t^3}{4n^3}, \tag{40}$$

$$k_{D,partial} = \frac{12EI_3}{n^3}\frac{sn+EI_3}{sn+4EI_3} = \frac{Et^3}{1-\nu^2}\frac{Et^3+12ns(1-\nu^2)}{4n^3(Et^3+3ns(1-\nu^2))}, \tag{41}$$

where $n = 0.5\cdot(b-p)$. The effect of shear deformability of the plate can be included in beams 2 and 3 as discussed in Section 3.2.2.

3.4. Case 2: Face plate loaded in tension or compression by horizontal plate

This case is presented in Fig. 3(e) and Fig. 7(c), where the face plate is centrically loaded by a horizontal plate of width b_{hp} and thickness t_{hp}. The previous formulation can be applied, but with c taken as $t_{hp}+t$, and $n = 0.5\cdot(b-b_{hp})$. The stiffness k_3 can be obtained from Eqs. (39) to (41). The effect of shear can be considered as indicated in section 3.2.2.

Table 6
Results of parametric study for face plate loaded by a horizontal plate.

Boundary condition	Statistic	Neves	Proposal	
		K_N/K_{FE}	K_C/K_{FE}	$K_{C,V}/K_{FE}$
Fixed (48 cases)	Max	2.102	2.004	1.411
	Min	0.987	0.881	0.871
	Mean	1.093	1.020	0.983
	C.o.V.	17.04%	17.46%	9.16%
	R^2	0.017	0.218	0.867
Pinned (48 cases)	Max	1.290	0.958	0.871
	Min	0.621	0.630	0.626
	Mean	0.723	0.782	0.776
	C.o.V.	16.45%	9.19%	8.93%
	R^2	0.932	0.978	0.961
Partial fixity ρ = 0.5, 1, 2 (144 cases)	Max	1.414	1.311	1.036
	Min	0.810	0.743	0.735
	Mean	0.930	0.874	0.860
	C.o.V.	10.40%	8.85%	6.48%
	R^2	0.942	0.994	0.996
All (240 cases)	Max	2.102	2.004	1.411
	Min	0.621	0.630	0.626
	Mean	0.921	0.885	0.867
	C.o.V.	18.52%	14.62%	10.80%
	R^2	0.975	0.997	0.998

3.5. Case 3: Face plate loaded in tension or compression by fin plate

This case is presented in Fig. 3(f) and Fig. 7(d), in which the face plate is centrically loaded by a fin plate of height h_{fp} and thickness t_{fp} in tension or compression. The model developed in the previous sections can be applied, with the following nuances: first, there is only one longitudinal beam (beam 1), and its effective width e can, for simplicity, be assumed equal to b; second, for this longitudinal beam 1 the model presented in Fig. 9 applies, assuming that the fin plate is rigid in its plane; third, for the transverse beam (beam 4) the model presented in Fig. 7(g) applies, with $n = b/2$, and a total load Q, leading to the following simplified equations:

$$k_{D,pinned} = \frac{48EI_2}{b^3} = \frac{E}{1-\nu^2}\frac{4t^3}{b^3}, \tag{42}$$

$$k_{D,fixed} = \frac{192EI_2}{b^3} = \frac{E}{1-\nu^2}\frac{16t^3}{b^3}, \tag{43}$$

$$k_{D,partial} = \frac{192EI_2(2EI_2+bs)}{b^3(8EI_2+bs)} = \frac{E}{1-\nu^2}\frac{8t^3[Et^3+6sb(1-\nu^2)]}{b^3[2Et^3+3sb(1-\nu^2)]}. \tag{44}$$

From these stiffness values, application of the model shown in Fig. 9 is similar to case C discussed in Section 3.2, see Fig. 8(c). Therefore, Eq. (18), with $e \le b$ can be used to find EI_1, λ is found by Eq. (19) replacing k_2 with $k_4 = k_D$, and Eq. (27) can be reformulated as:

$$K = 8EI_1\lambda^3 + k_4\, c, \tag{45}$$

where c is defined in Fig. 7(c) and can be adopted as $c = h_{fp}$ for simplicity. The effect of shear deformability of the plate can be included as discussed in section 3.2.2. The shear deformability for beam 4 is formulated as:

$$d_{D,V} = \frac{Qb}{4GA_v}, \tag{46}$$

and the total stiffness including bending and shear can be found by application of Eq. (31).

3.6. Summary of expressions

Table 2 presents a summary of the equations to estimate the initial stiffness of a face plate component subjected to transverse load (tension or compression), for the cases discussed above.

4. Validation of the proposed model

In this Section, the proposed models are validated with a set of recent

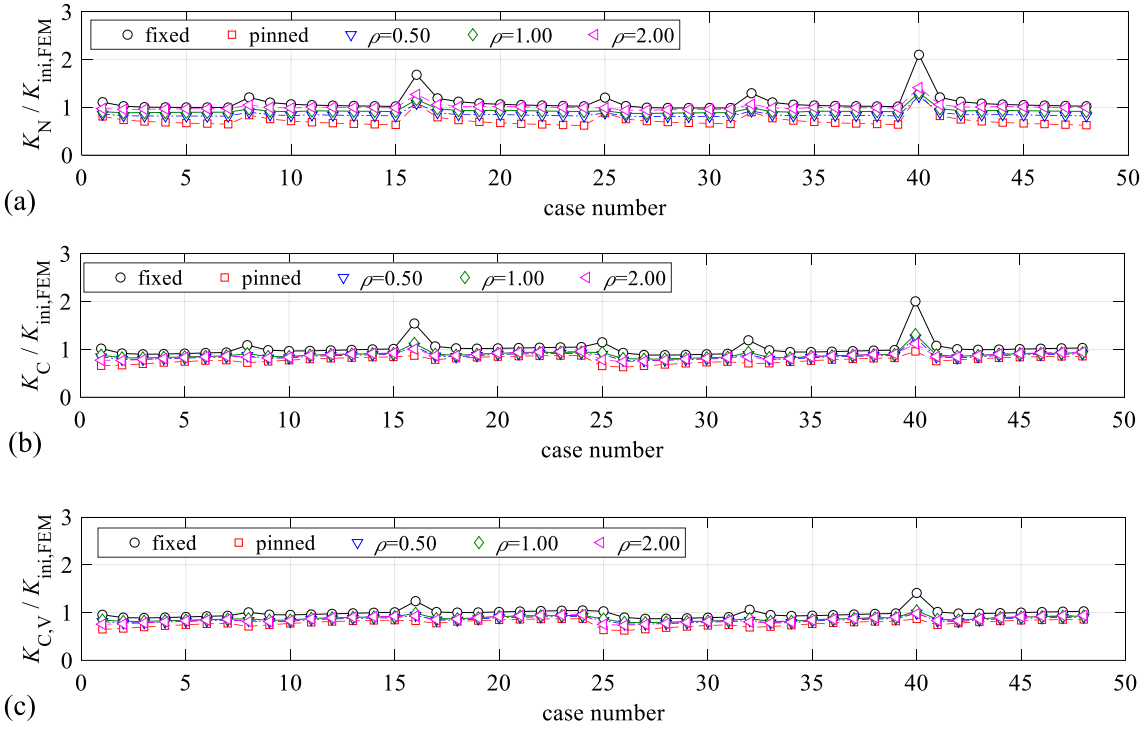

Fig. 14. Verification of the proposed methods for face plate loaded by a horizontal plate: (a) K_N; (b) K_C; (c) $K_{C,V}$.

Table B2
Parametric study cases – face plate loaded by fin plate.

n	t (mm)	b (mm)	h_p (mm)	b/t	h_p/b
1	10	100	50	10	0.50
2	10	150	75	15	0.50
3	10	200	100	20	0.50
4	10	250	125	25	0.50
5	10	300	150	30	0.50
6	10	350	175	35	0.50
7	10	400	200	40	0.50
8	10	450	225	45	0.50
9	10	500	250	50	0.50
10	10	100	100	10	1.00
11	10	150	150	15	1.00
12	10	200	200	20	1.00
13	10	250	250	25	1.00
14	10	300	300	30	1.00
15	10	350	350	35	1.00
16	10	400	400	40	1.00
17	10	450	450	45	1.00
18	10	500	500	50	1.00
19	10	100	200	10	2.00
20	10	150	300	15	2.00
21	10	200	400	20	2.00
22	10	250	500	25	2.00
23	10	300	600	30	2.00
24	10	350	700	35	2.00
25	10	400	800	40	2.00
26	10	450	900	45	2.00
27	10	500	1000	50	2.00

Table 7
Results of parametric study for fin plate.

Boundary condition	Statistic	Neves	Proposal	
		K_N/K_{FE}	K_C/K_{FE}	$K_{C,V}/K_{FE}$
Fixed (27 cases)	Max	1.308	1.193	1.145
	Min	0.987	1.045	1.009
	Mean	1.090	1.111	1.088
	C.o.V.	7.81%	3.17%	3.62%
	R^2	0.888	0.979	0.997
Pinned (27 cases)	Max	1.047	1.020	1.019
	Min	0.712	0.920	0.919
	Mean	0.824	0.989	0.984
	C.o.V.	9.71%	2.20%	2.42%
	R^2	0.986	0.999	0.998
Partial fixity	Max	1.240	1.079	1.064
$\rho = 0.5, 1, 2$	Min	0.854	0.919	0.918
(81 cases)	Mean	1.011	1.019	1.010
	C.o.V.	8.14%	2.35%	2.32%
	R^2	0.969	0.999	1.000
All (135 cases)	Max	1.308	1.193	1.145
	Min	0.712	0.919	0.918
	Mean	0.989	1.032	**1.020**
	C.o.V.	12.17%	4.75%	**4.36%**
	R^2	0.989	0.999	1.000

experimental results. This validation is further extended by comparison with the results of a parametric study carried out with high-quality FE models. In both cases, the agreement was good, surpassing the current existing expressions. The proposed model is also compared with the Neves model. It is not compared with the other methods reviewed in the state-of-the-art because they were only validated for tubular sections.

4.1. Verification of the FE models

4.1.1. Description of the FE models

To enable the full characterization of the plate behavior and its components, detailed finite element models (FEM) were developed in Abaqus [4], as shown in Fig. 10. The modelled plates have a width b and a length L equal to $4b$, except for the models representing the fin plate case, for which L is taken as $h_{fp} + 4b$. The adopted value of L was defined from a sensitivity analysis, in which it was shown that a value larger than $4b$ had negligible influence on the initial stiffness. Thus, the models represent well a plate of infinite length, a conclusion confirmed by other existing studies [14]. The double symmetry of the plate was considered, i.e., only a quarter of the plate was modelled with the appropriate symmetry boundary conditions.

The lateral edge of the plate was simply supported in-plane and in the out-of-plane directions, and linear rotational springs (about y, see Fig. 10) were included to simulate the support rotational stiffness. The spacing p_s between the springs was of the order of $2t$, with a rotational stiffness per spring $p_s \cdot s$. For the simply supported case ($s = 0$) and the fixed case ($s = \infty$) the springs were removed, and in the fixed case a rotational restraint was added. The top of the plate was free.

The FEA models were meshed with first-order 3D 8-node quadrilateral solid elements (C3D8RH), with reduced integration, hourglass control using the artificial stiffness method, and a hybrid formulation. A minimum of four elements were considered across the plate thickness, with a minimum 2 mm size of the element. The aspect ratio of the elements was controlled to vary between 1 and 3. A sensitivity analysis with different element types, mesh sizes and number of elements across the thickness was performed, leading to the options described, chosen to balance model size, computational time, and accuracy. Material and geometrical non-linearities were included in the model, although they hardly affect the value of the initial stiffness. The material was modelled as elastic-perfectly-plastic. The analysis was displacement-controlled with respect to a specified reference point located at the center of either the bolt or the loaded area.

The sensitivity analysis to determine the previously discussed model features was performed in the following way: a family of models was produced, in which only a certain parameter (for example, the plate length L) was varied and all other parameters were fixed. The force−displacement curve of all such models was compared, and the minimum value of the parameter producing no significant differences (i.e., less than 1%) in the response curve from the softest one was chosen. For instance, for L it was determined that no significant difference in results was obtained if L was larger than $4b$. This process was repeated for: plate length, number of elements across thickness, size of element, and element type. The C3D8RH element was chosen because it enhances convergence and therefore reduces the computation time, while requiring less disk space when compared to elements without reduced integration.

4.1.2. Partial fixity at the supports

The rotational stiffness s_{beam} of the transverse beam (beam 2) for the simply supported case is:

$$s_{beam} = \frac{2EI_2}{b}, \tag{47}$$

and is the inverse of the rotation at the support for a simply supported beam of span b and stiffness EI_2, subjected simultaneously to unit hogging bending moments at both supports. The ratio ρ between the support stiffness and the beam stiffness, neglecting the shear deformability of the lateral beams, is:

$$\rho = \frac{s}{s_{beam}}. \tag{48}$$

In the parametric study, values of $\rho = s/s_{beam} \approx [\infty, 2, 1, 0.5, 0]$ are adopted, deemed to represent appropriately the range of real rotational restraints; the first and last cases are exact and correspond to fixed support and pinned support, respectively.

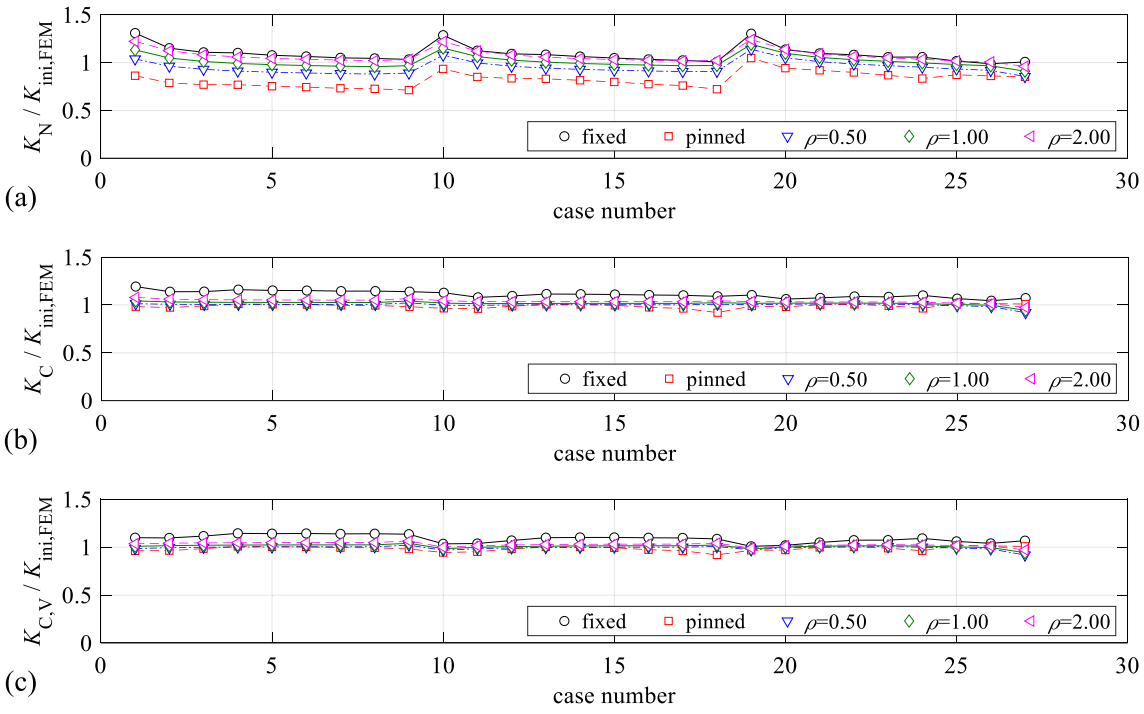

Fig. 15. Verification of the proposed methods for fin plates: (a) K_N; (b) K_C; (c) $K_{C,V}$.

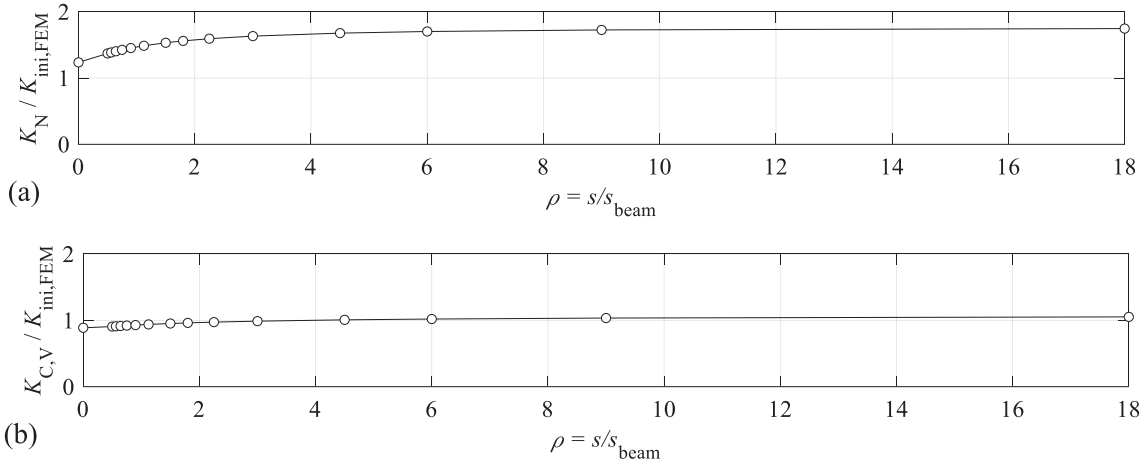

Fig. 16. Variation of the expressions' accuracy with support stiffness for face plate loaded by bolt row in tension: (a) K_N; (b) $K_{C,V}$.

4.2. Validation against experimental results

Table 4 compares the results of the proposed model against some recent experimental results carried out at the University of Coimbra [18] to study the response of the web/chord/face in both open and tubular columns, including welded and hot-rolled profiles, subjected to out-of-plane tension. The tests included the four open sections (3 rolled & 1 welded girder) shown in Fig. 11, that featured connections with single and double bolt rows with variable pitch and gauge distances.

The values of the normalized stiffness ρ of the test prototypes were recalculated as follows: First, advanced FEA models of the test specimens, reported elsewhere [19], were produced and calibrated with the experimental results. An excellent match was observed in terms of web panel displacements and force–displacement curves between the numerical models and the experimental values (measured by Digital Image Correlation) for the same applied total force F. Then, a simple plate model corresponding to the flat part of the web with uniform support rotational stiffness s, was produced, and the value of s was iteratively adjusted until the displacement u of the detailed model under the applied force F was matched. Finally, the models presented in sections 3.2 ($K_{C,V,flexible}$) and 3.3 ($K_{C,V,rigid}$) were applied, with the as-measured geometrical values and support rotational stiffness s as derived in the previous step. For the cases with two bolt-rows, the rigid segment at the center of beam 1 was taken with a length (in mm) $c = 90 + d_m$. The Neves model was also applied, with $d = p + d_m$ and $c = d_m$ (single bolt row) or $90 + d_m$ (two bolt rows). Table 3 shows the results. The actual stiffness of the connection lies between the stiffnesses predicted by the flexible and rigid end plate models, but in general closer to the latter. The results show a good match between the proposed model and the experimental results, while the Neves model shows a very poor match.

4.3. Validation against FE models

4.3.1. Parametric study. Face plate loaded by an infinitely flexible bolted end plate

The results for the initial stiffness obtained with the proposed

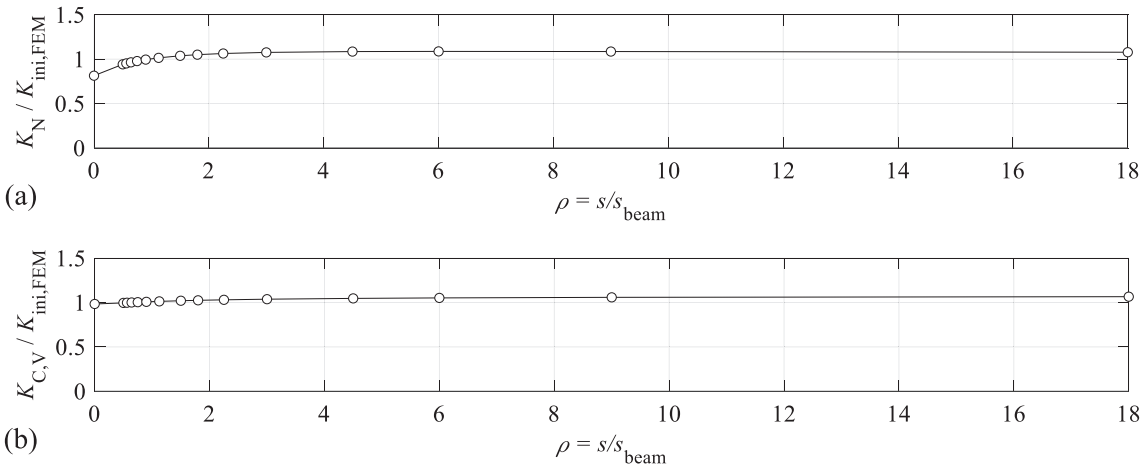

Fig. 17. Variation of the accuracy of the expressions with support stiffness for face plate loaded by fin plate in tension: (a) K_N; $K_{C,V}$.

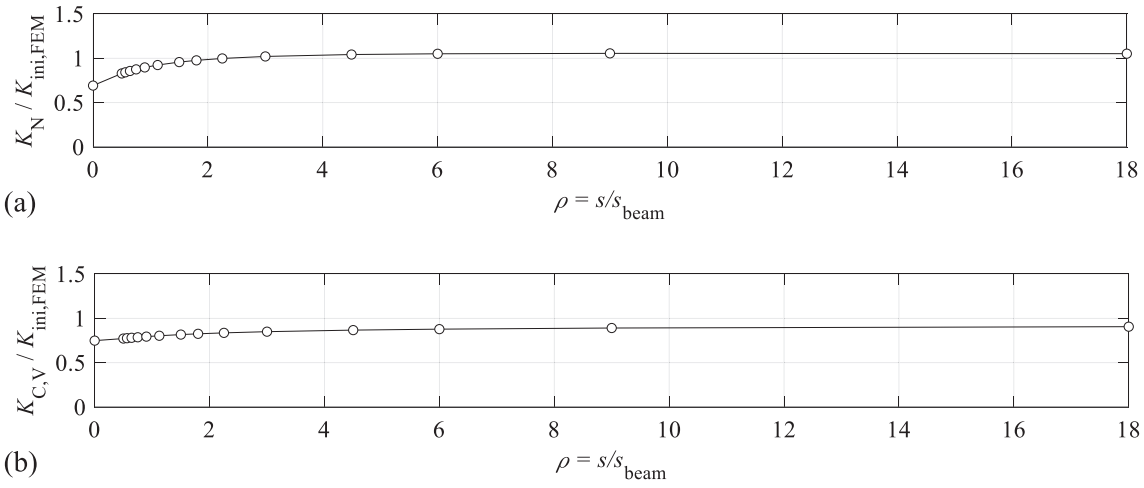

Fig. 18. Variation of the accuracy of the expressions with support stiffness for face plate loaded by horizontal plate in tension: (a) K_N; (b) $K_{C,V}$.

Table 8
Influence of the support stiffness for different cases.

		$K_{C,V}/K_{FE}$	K_N/K_{FE}
Face plate loaded by bolt row in tension	Mean	0.967	1.542
	C.o.V	5.90%	10.14%
Face plate loaded by fin plate in tension	Mean	1.026	1.018
	C.o.V	2.68%	7.31%
Face plate loaded by horizontal plate in tension	Mean	0.905	0.944
	C.o.V	6.80%	11.10%

equivalent grid model were compared to those of FE analyses for 240 different cases representing usual configurations of bolts on a face plate, with different boundary conditions. The rotation of the load application area was not restrained, simulating an infinitely flexible end plate (Case 1a). For all cases $E = 210\text{kN/mm}^2$, $\nu = 0.3$, $d = 16$ mm, $d_m = 28.4$ mm. Three values of the plate thickness t were adopted (8 mm, 12 mm, 16 mm), corresponding to ratios t/d of (0.50, 0.75, 1.00), respectively. Two different values of p (80 mm, 96 mm) were included, resulting in p/d ratios of 5 and 6, respectively. For each plate thickness, 9 values of slenderness b/t (10, 15, 20, 25, 30, 35, 40, 45, 50) were considered. These values correspond to the usual range of face plate slenderness. Some values of b resulting in unrealistic constructive conditions were eliminated (small widths not capable of accommodating the two bolts

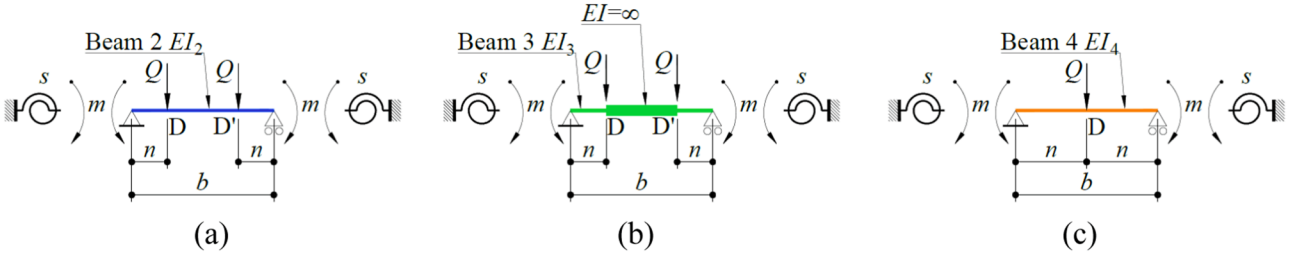

Fig. A1. Compatibility equations for transverse beams.

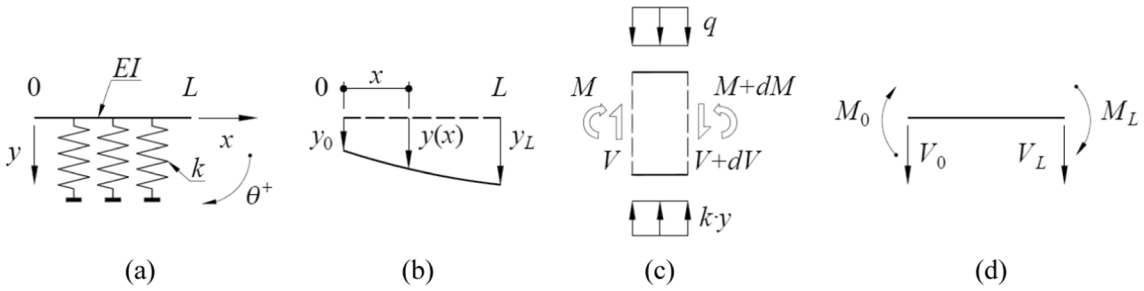

Fig. A2. Compatibility equations for transverse beams.

with proper edge distances and spacings). These options resulted in 48 different representative cases, listed in Annex B (Table B.1), analyzed for three different boundary conditions, namely: fixed (48 cases), pinned (48 cases) and partial fixity (3 values of partial fixity, 3 × 48 = 144 cases). The initial stiffness K_{FEA} was obtained at the first load step of the analysis. It was compared with the average of the secant stiffness calculated for the first 5 steps and found to be practically identical. The initial stiffness according to the proposed method neglecting shear (K_A, K_B, K_C), and considering shear deformation ($K_{A,V}$, $K_{B,V}$, $K_{C,V}$) were calculated adopting for simplicity $e = b/2$ (further refinement of this parameter is possible). Additionally, the stiffness was calculated with the Neves formulation (K_N), Eq. (2), for comparison purposes, although this expression is not strictly applicable to this case, as it assumes a rigid behavior of the plate between bolts. The ratio K_X/K_{FEA} was obtained, where K_X refers to any of the previously listed stiffness values (A, B, C, AV, BV, CV, N). A value of $K_X/K_{FEA} = 1$ indicates that the proposed method is accurate, whereas values larger or smaller than 1 indicate overprediction or underprediction of the stiffness, respectively.

Fig. 12(a)−(c) presents K_X/K_{FEA} for the whole set and 3 methods (K_N, K_C, $K_{C,V}$). In each sub-plot, vertically aligned points correspond to the same combination of geometrical parameters and different values of ρ. The vertical scale of the figures is the same to facilitate the comparison between results. Statistics for K_X/K_{FEA} are shown in Table 4, including the R^2 values of the proposed methods (for the Neves method R^2 results in negative values, corresponding to worse predictions than the baseline [20], highlighting the poor performance of the method). These results show a good agreement between the stiffness values predicted by the proposed methods and those obtained by the FEA model. The best expression to approximate the results is $K_{C,V}$, Eqs. (18)−(19), for which $K_{C,V}/K_{FEM}$ presents a mean value of 0.973 and a coefficient of variation of 8.8%. Regarding this expression, the method tends to underpredict the stiffness values for the pinned case and to overpredict for the fixed case. The expression follows clear trends but with some unexpected results, such as those presented for cases 16 and 40, that correspond to very low values of b/t and n/t, for which torsional components of the plate behavior can be very relevant. The dispersion of the predictions (measured by the C.o.V.) is very moderate, so the expressions provide a consistent level of accuracy across the whole range of cases under study.

4.3.2. *Parametric study. Face plate loaded by an infinitely stiff bolted end plate*

The same cases defined for the previous study were used to simulate a face plate loaded by an infinitely stiff bolted end plate, simply by restraining the rotation of the load application area. Only the most accurate expressions K_C and $K_{C,V}$ were considered. The results, shown in Table 5 and Fig. 13, indicate that the proposed method gives good results and exhibits a much smaller scatter of the results when compared to the Neves model, Eq. (2), (14.9% vs 45.1%) and leads to safe sided results, in contrast to the Neves model that highly overestimates the initial stiffness. The R^2 values confirm the accuracy of the proposed model.

4.3.3. *Parametric study. Face plate loaded by a horizontal plate*

The cases considered for the verification of the face plate loaded by a horizontal plate are the same as for the previous case, but the width of the horizontal plate is taken as $b_{hp} = b$, and the thickness of the horizontal plate is assumed constant with $t_{hp} = 8$ mm. The corresponding results are listed in Table 6 and Fig. 14, showing average values similar to those obtained with the Neves model, Eq. (2), but with a consistent reduction in variability and better R^2 values.

4.3.4. *Parametric study. Face plate loaded by a fin plate*

The initial stiffness values obtained with the proposed method were compared to those of FEA for different cases representing usual configurations of fin plates attached to face plates, with different support conditions. For all cases $E = 210\text{kN/mm}^2$, $\nu = 0.3$, $t = t_{fp} = 10$ mm; nine different values of slenderness b/t were adopted (10, 15, 20, 25, 30, 35, 40, 45, 50), resulting in nine values of b (100, 150, 200, 250, 300, 350, 300, 450, 500) (mm); three different ratios of h_{fp}/b (0.50, 1, 2) were considered; e was consistently taken as b. These options resulted in 27 different representative cases, listed in Annex B (Table B.2), analyzed under three different boundary conditions, namely: fixed (27 cases), pinned (27 cases) and partial fixity (3 values of partial fixity, 3 × 27 = 81 cases). In these results e has been taken as b. Overall (see Table 7 and Fig. 15), the new expression provides consistent accuracy and dispersion across the whole range of boundary conditions, improving the predictions of the Neves model, Eq. (2), for all cases, with an excellent R^2 value.

4.3.5. *Influence of support stiffness on the accuracy of the expressions*

The influence of the support stiffness is studied for one single case with the three main loading forms previously discussed. The selected dimensions for a face plate loaded by a bolt row in tension and a horizontal plate in tension are $b = 300$ mm, $t = 12$ mm. Additionally, for the face plate loaded by a bolt row in tension, $p = 96$ mm, $d = 16$ mm, $d_m = 28.4$ mm, and for the face plate loaded by a horizontal plate in tension $t_{hp} = 8$ mm, $b_{hp} = 96$ mm. The selected dimensions for a face plate loaded by a fin plate in tension are $b = 250$ mm, $t = 10$ mm, $h_{fp} = 250$ mm, $t_{fp} = 10$ mm. The following 16 support stiffness values are studied: ρ = [0 (pinned), 0.50, 0.56, 0.64, 0.75. 0.90, 1.13, 1.50, 1.80, 2.25, 3, 4.5, 6, 9, 18, ∞ (fixed)]Section 4.1.2.

For the face plate loaded by a bolt row in tension the results of $K_{method}/K_{ini,FEM}$ are shown in Fig. 16. Fig. 17 shows the results for the face plate loaded by a fin plate in tension, and Fig. 18 displays the results for the face plate loaded by a horizontal plate in tension. Statistics across all values of support stiffness considered in each case are summarized in Table 8. The results show that the average differences between the models and the numerical values are small for both methods (except for the Neves model in case of a bolt row loaded in tension), but the dispersion for the proposed method is much lower. This results from the empirical nature of the Neves model in terms of the width of the equivalent beam strip, unlike the proposed method that uses a 2D (grid) model to account for the contributing width. Furthermore, since most real cases of steel joints exhibit small support stiffness, with values of ρ < 5 (see Table 3, where all cases present a value of ρ below 5 and two cases even have values of 0.3 and 0.8), Fig. 16 to Fig. 18 show a much better agreement of the numerical results with the proposed method (Eq.

(2)).

5. Conclusions

The face plate is a joint component that appears in common engineering practice, for instance in weak-axis connections of beams to open-section columns, or in connections to tubular columns. Despite its frequent occurrence, the component is not codified. This paper proposes a model for the estimation of the initial stiffness of the face plate subjected to out-of-plane tension, as a first step towards its complete characterization. The model is based on a simplified grid in which a main beam in the face plate longitudinal direction is continuously supported by transverse beams and leads to relatively simple closed-form analytical solutions (summarized in Table 2), for loading produced by very rigid or very flexible bolted end plates in tension, horizontal plates in tension or compression, and fin plates in tension or compression. The predictions obtained by the model have been checked against those obtained with finite elements for a large dataset of realistic cases. The method provides a good estimate of the initial stiffness and a very low dispersion across the cases considered. Comparison with experimental results for bolted end plates indicates that the proposed method for flexible and rigid end plates provides suitable lower and upper bounds of the actual connection stiffness.

CRediT authorship contribution statement

Jorge Conde: Conceptualization, Methodology, Formal analysis, Writing – original draft, Writing – review & editing. **L. Simões da Silva:** Supervision, Conceptualization, Methodology, Writing – original draft, Writing – review & editing. **Ana Francisca Santos:** Software, Investigation, Writing – review & editing. **Melaku S. Lemma:** Software, Investigation, Formal analysis, Writing – original draft, Writing – review & editing. **Trayana Tankova:** Conceptualization, Writing – review & editing.

Declaration of Competing Interest

The authors declare that they have no known competing financial interests or personal relationships that could have appeared to influence the work reported in this paper.

Data availability

Data will be made available on request.

Acknowledgments

This work was partly financed by:

- FCT / MCTES through national funds (PIDDAC) under the R&D Unit Institute for Sustainability and Innovation in Structural Engineering (ISISE), under reference UIDB / 04029/2020, and under the Associate Laboratory Advanced Production and Intelligent Systems (ARISE) under reference LA/P/0112/2020.
- Grant with reference UP2021-035 (RD 289/2021) from "Ministerio de Universidades de España", funded by European Union, NextGenerationEU, attributed to the second author.
- The doctoral grant 2020.07414.BD by the Portuguese Foundation for Science and Technology (FCT) attributed to the fourth author.

Appendix A:. Derivations

A.1 Stiffness of elastic foundation (transverse beams)

The elastic foundation stiffness of the adopted grid model is calculated as the stiffness of beams 2, 3 and 4 at the point of load application, and can be easily derived using the compatibility method. Consider the beams displayed in Fig. 7(e)–(g). The compatibility method can be applied, dividing the beam from the supporting springs as shown in Fig. A1(a)–(c). In all cases, the rotation of the unit spring at the left side θ_s is:

$$\theta_s = -m/s, \tag{A.1}$$

where m (kN·mm/mm) is the internal bending moment, considered positive as displayed (whereas θ is considered positive if counterclockwise), and s (kN/rad) is the support partial stiffness. Focusing on Fig. A1(a), the corresponding rotations at the left side of the simply supported beam for are:

$$\theta_v = [-Qn(b-n)/2 + mb/2]/EI_2, \tag{A.2}$$

where Q (kN/mm) is the applied load per unit length. Equating both expressions:

$$m = \frac{Qns(b-n)}{bs + 2EI_2}, \tag{A.3}$$

and the corresponding displacement at point D can be calculated using the superposition principle as:

$$d_{\mathrm{D,partial}} = Q\frac{sn^3(2b-3n) + 2EI_2n^2(3b-4n)}{6EI_2(2EI_2 + bs)}, \tag{A.4}$$

whereupon Eq. (17) is derived as $Q/d_{\mathrm{D,partial}}$. Eqs. (15) and (16) are found specializing Eq. (A.4) for $s = \infty$ and $s = 0$, respectively, and replacing EI_2 by Eq. (14).

Beam 4 shown in Fig. A1(c) can be seen as a particular case of these equations for $n = b/2$, with half the load (Q instead of $2Q$), resulting in Eqn. (44), which can be specialized for $s = \infty$ and $s = 0$, to render Eqs. (42) and (43), respectively.

Finally, for the case shown in Fig. A1(b), the corresponding equations are:

$$\theta_v = \left[-Qn^2/4 + mn\right]/EI_3, \tag{A.5}$$

$$m = \frac{Qn^2s}{4(ns + EI_3)}, \tag{A.6}$$

$$d_{\mathrm{D,partial}} = Q\frac{n^3(8EI_3 + 5ns)}{24EI_3(EI_3 + ns)}, \tag{A.7}$$

A.2 Stiffness of main beam (beam 1)

Beam 1 can be represented as an infinite member supported by an elastic foundation whose stiffness k is that of beam 2, 3 or 4, Fig. A2. The differential equation for the displacement $y(x)$ of a beam with stiffness EI on an elastic foundation of stiffness k under distributed load q is [34]:

$$EI\frac{d^4y}{dx^4} + ky - q = 0. \tag{A.8}$$

The homogeneous counterpart of this equation ($q = 0$) admits the following explicit solution:

$$y = \exp[\lambda x](C_1\cos\lambda x + C_2\sin\lambda x) + \exp[-\lambda x](C_3\cos\lambda x + C_4\sin\lambda x), \tag{A.9}$$

where exp[·] is the exponential function, C_1 to C_4 are constants depending on boundary conditions and λ is the parameter relating the beam and foundation stiffnesses:

$$\lambda = \left(\frac{k}{4EI}\right)^{0.25}. \tag{A.10}$$

Eq. (A.9) can be solved explicitly for the three cases displayed in Fig. 8, using different assumptions, and taking $EI = EI_1$, $k = k_2$. For the force applied as a point load, Fig. 8(a), $y(\infty) = 0$; $y'(0^+) = 0$; $V(0+) = B/2$, which leads to Eq. (23). For the force applied as two point loads, Fig. 8(b), the solution can be found superimposing the solutions for two point loads at $\pm d_m/2$, leading to Eq. (26). Finally, for the force applied as two point loads with infinite stiffness in between, Fig. 8(c), the stiffness of the central part, $k_2{\cdot}d_m$, is added, resulting in Eq. (27).

Appendix B:. Description of parametric studies

B.1 Face plate loaded by bolted end plate and horizontal plate

Table B.1 defines the 48 basic cases included in the parametric studies described in Sections 4.3.1, 4.3.2, And 4.3.3. These 48 cases were then calculated with 5 different support conditions ranging from fixed to pinned, adding up to a total of 240 cases. The cases were used for the parametric study for a face plate loaded by an infinitely flexible end plate, an infinitely rigid end plate, and a horizontal plate, as described in the main text.

B.2 Fin plate

Table B.2 defines the 27 basic cases included in the parametric study described in Section 4.3.4 These 27 cases were calculated with 5 different support conditions ranging from fixed to pinned, adding up to a total of 135 cases.

References

[1] En,. Eurocode 3: Design of steel structures – part 1–8: design of joints. Brussels, Belgium: European Committee for Standardization; 1993-1-8 (2005)..
[2] FprEN 1993-1-8 (2022). Eurocode 3: Design of steel structures – part 1-8: Joints. Brussels, Belgium: European Committee for Standardization.
[3] Simões da Silva L. Towards a consistent design approach for steel joints under generalized loading. J Constr Steel Res 2008;64(9):1059–75.
[4] Simulia, Abaqus User Manual, Dassault systems Simulia Corp.; 2021. https://help.3ds.com/HelpProductsDS.aspx [last accessed 06/01/2023].
[5] Hetényi M. Beams on elastic foundation. The University of Michigan Press; 1946.
[6] Timoshenko S. Strength of materials. 2nd ed. New York: D. Van Nostrand Company; 1940.
[7] Neves LC. Static monotonic and cyclic behavior of minor axis and tubular joints in steel and composite structures (in Portuguese). University of Coimbra; 2004. PhD Thesis.
[8] Neves LC. Semi-rigid behaviour of beam-to-column minor-axis joints (in Portuguese). University of Coimbra; 1996. MSc Thesis.
[9] Jaspart JP, Pietrapertosa C, Weynand K, Busse E, Klinkhammer R, Grimault JP. Development of a full consistent design approach for bolted and welded joints in building frames and trusses between steel members made of hollow and/or open sections-application of the component method. Appl Compon method Draft Final Rep 2005;1.
[10] Park AY, Wang YC. Development of component stiffness equations for bolted connections to RHS columns. J Constr Steel Res 2012;70:137–52. https://doi.org/10.1016/J.JCSR.2011.08.004.
[11] Park AY. Semi-rigid joints to tubular columns and their use in semi-continuous frame design; 2012.
[12] Szilard R. Theories and applications of plate analysis: classical, numerical and engineering methods. John Wiley & Sons; 2004.
[13] Garifullin M, Bronzova M, Pajunen S, Mela K, Heinisuo M. Initial axial stiffness of welded RHS T joints. Elsevier; 2019.
[14] Ghobarah A, Mourad S, Korol RM. Moment-rotation relationship of blind bolted connections for HSS columns. J Constr Steel Res 1996;40:63–91. https://doi.org/10.1016/S0143-974X(96)00044-2.
[15] Mahmood M, Tizani W. A component model for column face in bending of extended HolloBolt connections. J Constr Steel Res 2021;182:106655. https://doi.org/10.1016/j.jcsr.2021.106655.
[16] Hillerborg A. Strip method of design. Cement and Concrete Association 1974.
[17] Reddy JN. Theory and analysis of elastic plates. Taylor and Francis; 1999.
[18] Lemma MS, Silva LS, Rebelo C. Experimental campaign: column web/face characterization under out-of-plane and transverse loads [internal test report]. Portugal: University of Coimbra; 2023.
[19] Lemma MS, Silva LS, Conde J, Rebelo C. Experimental and numerical studies on characterization of column webs/faces loaded out-of-plane in steel joints. Internal Report. Portugal: University of Coimbra; 2023.
[20] Draper NR, Smith H. Applied regression analysis. Wiley-Interscience; 1998.